AAPM REPORT NO. 118

Parallel Imaging in MRI: Technology, Applications, and Quality Control

The Report of AAPM Task Group 118

June 2015

This page intentionally left blank.

Parallel Imaging in MRI: Technology, Applications, and Quality Control

The Report of AAPM Task Group 118

Nathan Yanasak[1], TG Chair, Geoff Clarke[2], former TG Chair,
R. Jason Stafford[3], Frank Goerner[4,5], Michael Steckner[6],
Ishtiaq Bercha[7], Joseph Och[8], and Maxwell Amurao[9]

1Department of Radiology and Imaging, Georgia Regents University, Augusta, GA 30912
[2]Department of Radiology, University of Texas Health Science Center, San Antonio, TX 78249
[3]Department of Imaging Physics, University of Texas MD Anderson Cancer Center, Houston, TX 77030
[4]Dept of Radiology, University of Texas Medical Branch, Galveston, TX 77555
[5]Department of Radiology and Medical Imaging, University of Virginia, Charlottesville, VA 22908
[6]Toshiba Medical Research Institute, Vernon Hills, IL 60061
[7]Department of Radiology, University of Colorado, Aurora, CO 80045
[8]Department of Medical Health Physics, Geisinger Medical Center, Danville, PA 17822
[9]Department of Radiology, Columbia University, New York, NY 10032

ISBN: 978-1-936366-47-7
ISSN: 0271-7344

Published by

American Association of Physicists in Medicine
One Physics Ellipse
College Park, MD 20740-3846

Contents

Abstract

The field of magnetic resonance imaging has been undergoing a transformation during the past decade, with a growing emphasis on characterizing disease using imaging metrics of more direct physiological relevance, i.e., quantitative imaging biomarkers. As a result, the complexity of clinical magnetic resonance imaging techniques and the availability of new image sequences have increased dramatically in search of these biomarkers. Two critical challenges have emerged during this transformation: 1) how does the clinic acquire increased amounts of imaging data within a clinically reasonable amount of time? and 2) how does the physician assess this increased volume of data in a time-efficient manner? To address the first challenge, parallel imaging (pMRI) was developed as a class of image acquisition and reconstruction schemes that serves to increase the amount of imaging data acquired within a given time. While the use of pMRI is becoming widespread clinically, the complexity of the technique can lead to corrupted, nondiagnostic images if not utilized properly. This document is the report from Task Group 118, formed in order to help educate the medical physicist about the technique of pMRI, and about how this technique can affect image characteristics. Important topics that are addressed within this document are clinical uses of pMRI, artifacts, and properties of phased-array coils (which are strictly required in pMRI). This report also enumerates and describes specific quality assurance concerns that arise with the use of pMRI, although a comprehensive treatment of pMRI-based QA procedures is beyond the scope of this report.

Preamble

Task Group 118 of the American Association of Physicists in Medicine was established to describe the basis of parallel imaging in magnetic resonance imaging (MRI) and its applications to the medical physics community. This document is the final result of numerous discussions and written drafts in pursuance of this goal. Understanding the technology of parallel imaging has become important recently as certain protocols that routinely employ it are gaining in popularity. Because it often reduces the number of radio frequency (RF) pulses used in a study, parallel imaging has distinct advantages for reducing specific absorption rate (SAR). This feature is particularly advantageous for higher field strengths, which is the fastest-growing sector of the MRI system market.

The label of parallel imaging, or pMRI, refers to a class of image acquisition and reconstruction schemes that can produce more images using fewer excitations than one would acquire with conventional Fourier-transform MRI. The typical MRI scanning paradigm uses phase-encoding magnetic field gradients to reveal the spatial location of signals received in a coil. This approach is, in part, replaced with a new paradigm that exploits the differences in the spatial sensitivity of multiple coil elements receiving in parallel to localize signal in a manner that is independent of phase-encoding. The value of this strategy is that it can provide the clinician improved imaging performance.

The essential improvement available using pMRI is faster image acquisition, and the benefits that may result include decreased motion artifact, reduced breath-hold time, shorter durations of diagnostic exams, and an increase in the number of series per exam. Fewer phase encodings also leads to some decrease of the signal-to-noise ratio for many applications, and the reconstruction methods employed may require a change in our understanding of the basic nature of signal-to-noise ratios. In specific imaging schemes, such as echo-planar imaging and fast spin echo protocols, pMRI allows a shorter readout duration that can improve image quality in other ways, such as improved geometric fidelity, higher spatial resolution, and reduction of susceptibility distortions. One can also choose to increase scanning resolution for an exam of a given duration.

However, pMRI methods are not free of problems, including unique artifacts that the imaging physicist must learn to recognize and control. Thus, while pMRI enhances the clinical utility of MRI, achieving these benefits requires the extra cost of increasing the technical complexity of the MR system. Therefore, the medical physicist must successfully navigate through the complex and murky waters of this novel technology. Several questions are important to consider. For example, what protocols may benefit from the use of pMRI? How can the particular design of a coil (or the RF system in general) affect imaging performance? What are the advantages and disadvantages of using different pMRI schemes? Which image reconstruction and data transfer rates are necessary for efficient implementation of pMRI?

Considering these and many more questions, this report provides practical guidance and assistance for the medical physicist so that pMRI may be more readily applied and understood within this clinical environment. In Section 2, a review of spatial encoding using standard Fourier transform MRI and pMRI techniques is given. Next, a description of general and specific uses of pMRI is given in Section 3, followed by a discussion of coil array properties and their use in pMRI (Section 4). Image quality issues and concerns as they relate to pMRI are enumerated in Section 5, including an introduction to typical artifacts and important considerations specific to pMRI for maintaining quality assurance. Finally, Section 6 presents a variety of new pMRI advanced developments that may become routine in the near future.

1. Introduction and Overview

1.1 *k*-Space and Spatial Encoding in Magnetic Resonance Imaging

In the Fourier method of magnetic resonance imaging (MRI), the signal is generated by means of a radio frequency (RF) pulse[1]. As the signal evolves, three orthogonal linear magnetic field gradients, $G_x = \partial B_z / \partial x$, $G_y = \partial B_z / \partial y$, and $G_z = \partial B_z / \partial z$, are applied in succession (see a simplistic example in Figure 1). As an example of how the local magnetic field changes over time, the z-component of the field is given by:

$$B_z(r) = B_o + zG_z \quad for\ 0 < t < t_z \tag{1}$$

$$= B_o + yG_y \quad for\ t_z < t < t_z + t_y \tag{2}$$

$$= B_o + xG_x \quad for\ t_z + t_y < t \tag{3}$$

The MRI signal is sampled in the third time interval as a function of $t_x = t - (t_z + t_y)$. Although the MR signal is acquired while the G_x gradient is turned on, the MRI signal clearly depends on gradient contributions during the time intervals t_z and t_y. The effect of the gradients is to encode spatial information from the x-, y- and z-directions in the phase of the MRI signal. If the MRI signal is denoted as $S(t) = S(t_x,t_y,t_z)$, then the observed signal, S(t), can be written as:

$$S(t) = \iiint c(\mathbf{r})\, s(\mathbf{r},t)\, d\mathbf{r}\ , \tag{4}$$

where $s(\mathbf{r},t)$ is the signal from volume element $d\mathbf{r} = dx\, dy\, dz$, and $c(\mathbf{r}) = c(x,y,z)$ is the coil spatial sensitivity function. For the case of birdcage-type volume coils, $c(\mathbf{r})$ is fairly uniform throughout the imaging volume. Kumar, Welti, and Ernst[1] first described the three-dimensional (3D) Fourier transform of S(t) as a measure of the spatial spin density function, which comprises part of $s(\mathbf{r},t)$ in Equation 4. However due to limitations in computing at the time, Kumar et al. only implemented a two-dimensional (2D) version of their Fourier MR imaging method. MRI acquisitions often are con-

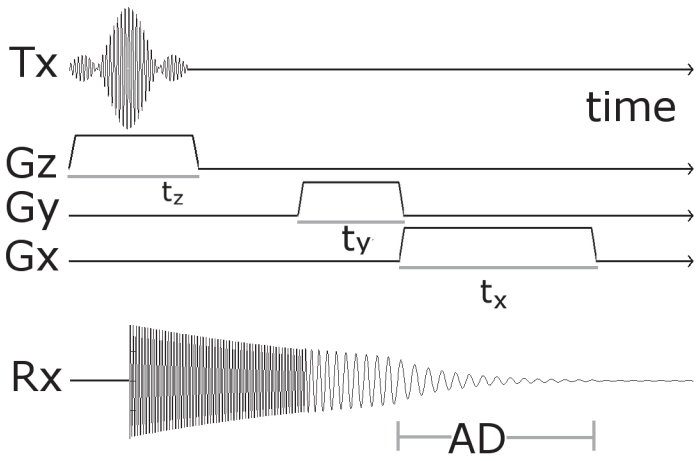

Figure 1. Basic pulse sequence diagram for Fourier MR imaging. TX and RX are the transmitter and receiver channels, respectively. The label "AD" denotes the time during which the analog-to-digital converter is turned on and the NMR signal is acquired.

strained to two dimensions, in which the signal from the third dimension is restricted to a limited slice using a selective excitation method[2]. For simplification, we will refer only to the 2D implementations in subsequent discussions, unless otherwise stated.

Refinements to the Fourier transform MR imaging method soon allowed production of clinically valuable images. In a "spin warp" imaging scheme[3], the encoding of spatial information with phase was performed successively by varying the amplitude of gradient pulses. Initially this was achieved by the application of a half-sine wave pulse, which was applied for the same time in each imaging cycle but with varying amplitude. Unlike the method described by Kumar et al.[1], in spin-warp imaging the phase-encoding gradient was applied for a constant time interval with the amplitude incremented with each successive excitation. Most of the MRI sequences in use today are based on spin-warp MR imaging and are generally known as Fourier-transform magnetic resonance imaging (FT-MRI) methods.

In FT-MRI the gradients, G_x, G_y, and G_z are time-varying and are used to map the spatial frequency domain content of the imaged object directly into the MRI signal. This mapping is conveniently described in the spatial frequency space, known as *k*-space[4,5]. A brief development of this concept follows.

Figure 2 depicts a simple gradient echo or field echo MRI pulse sequence with slice selection (or a "2D" sequence). While the ADC is turned on during signal acquisition, the frequency-encoding gradient (G_x) is also turned on. At a given time after G_x is turned on, *t*, the signal contribution from a local region (or "voxel") will have a particular signal phase that encodes its location. Prior to readout, the phase-encoding gradient, G_y, will also have encoded spatial information according to the duration of the phase-encoding gradient pulse, τ. Ignoring magnetization relaxation processes, the combined effects of both gradients on the local signal in this voxel is:

$$\Delta s(t) = \rho(x,y)\, exp(i\gamma x G_x t)\, exp(i\gamma y G_y \tau)\Delta x\, \Delta y. \quad (5)$$

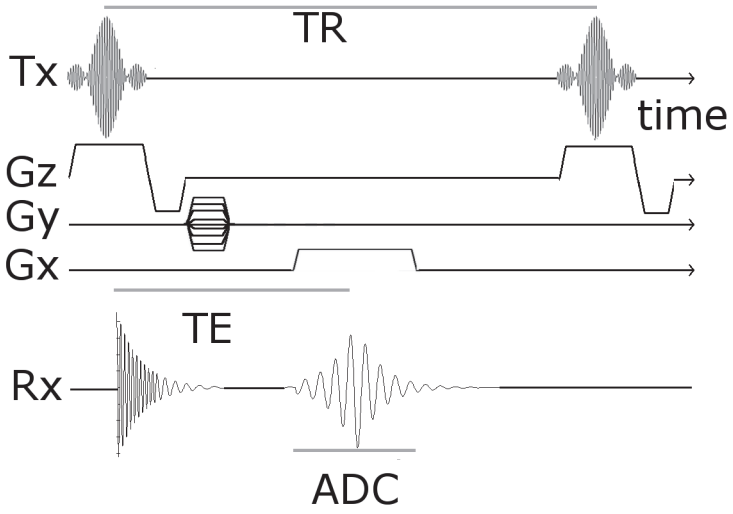

Figure 2. Practical implementation for Fourier MR imaging using the "spin warp" approach. The phase-encoding gradient (Gy) has multiple values indicating it is being successively incremented with each acquisition, which takes place following every excitation RF pulse repetition period (TR). The time-to-echo (TE) is defined as the time from the middle of the excitation pulse to the maximum signal. This maximum signal occurs when the center of *k*-space (zero spatial frequency) is sampled.

The spatial spin density function is denoted as ρ. If the gradient pulses can be idealized as rectangular pulses with instantaneous rise times, then the signal can be redefined simply in terms of its spatial frequency components, k_x and k_y:

$$k_x = \left(\gamma / 2\pi\right) G_x t \tag{6}$$

$$k_y = \left(\gamma / 2\pi\right) G_x \tau \tag{7}$$

Using this formalism, a particular time during readout defines a coordinate (k_x, k_y) in *k*-space. The data readout process involves sampling along trajectories in *k*-space that are controlled by time-varying gradients. Therefore, each phase encoding represents a particular trajectory through *k*-space. If, at a particular time during readout, we integrate the signal over the entire slice plane (assuming a voxel to be a differential volume element when considering Equation 5), the total signal in the *k*-space formalism becomes:

$$S(t) = \iint \rho(x,y)\, exp\left(i2\pi x k_x\right)\, exp\left(i2\pi y k_y\right) dx\, dy \tag{8}$$

Here, we are assuming uniform sensitivity in the receiver coil to all regions (i.e., c(x,y)≡1 in Equation 4). Equation 8 shows how the MRI signal has been encoded by the spatial frequency distribution of the original object. The decoding process involves inverse Fourier transformation to obtain an image that describes the original spatial distribution according to ρ(x,y). To reproduce accurately an image with a matrix of M x N voxels using conventional FT-MRI, the pulse sequence must execute enough phase-encoding steps to cover an array of M x N discrete positions in *k*-space along readout trajectories. In addition to describing signal encoding schemes, the *k*-space formulation has also been used to model spin excitation in MRI[6].

1.2 Early Parallel Magnetic Resonance Imaging (pMRI) Techniques

Parallel imaging methods use knowledge of the spatial distribution of signals received by multiple RF detectors (such as a surface coil in an array of these "elements") to replace some of the time-consuming phase-encoding steps in the MRI process. In this manner, signal is received from multiple coil elements "in parallel," and the sampling of fewer positions in *k*-space along readout trajectories (i.e., fewer phase encodings) is compensated by the duplicity of data from all coil elements. The first approach to pMRI, presented by Hutchinson, et al.[7], employed N surface coils arranged around the object, where N is the number of *k*-space lines to be acquired for an image. Kwiat, et al.[8] demonstrated a procedure called Combined Zeugmatography and Array (COZA) that was based on solving inverse source problems. Pulsed gradients were still used for slice selection and frequency encoding but the multiple information signals necessary for spatial encoding in the third dimension were obtained from signals recorded by different detection coils. In essence, phase encoding was replaced with distance encoding.

The problem of coupling in a system of a large number of closely spaced coils was noted for both methods. To create an N x N pixel image, the COZA method required N^2 closely packed RF coils, impractical to implement in a clinical setup. In addition, in a large multi-element array, the coil size must be small and the coupling between adjacent coils should be negligible. Signals sensed by adjacent detectors in high-resolution imaging can cause low SNR, leading to a singularity problem during decoding, which limits the practical use of the method.

A novel technique involving a multiple coil receiver system with a sub-encoding strategy was proposed by Ra, et al. to reduce scan time[9]. This method reduced the number of phase-encoding steps to be acquired by a factor L. The end result was an aliased image which was unfolded by using the dis-

tance-dependent sensitivity differences among L_c receiver coils where $L_c \geq L$. L_c could be a small number so that multiple coils could be designed to have a higher sensitivity with less decoupling. In this approach, the rate of reduction in data acquisition time was proportional to the number of receiver coils. Any given voxel in an aliased image resulting from sub-encoding is the sum of L voxels which are a certain distance apart from each other in the object. This approach reduces the singularity problem during spatial decoding: each coil has a different sensitivity to a given voxel depending on its position. This scheme offered flexibility in the number of coils regardless of the required image resolution, and it could be applied to any fast imaging method based on a modification of the pulse sequence.

Another simple approach put forward by Carlson et al.[10] involved two receiver coils, which acquired half the number of phase-encoding steps as in a standard MRI sequence. Spatial localization was based, in part, on standard phase encoding steps as well as on having multiple receivers. Coil coupling problems were partially mitigated by using receivers with no intrinsic coupling. One receiver was a common head or body coil, referred to as the primary coil, while the other one was a gradient response and is referred to as secondary channel. The sensitivity of this secondary channel coil was zero along the center of phase encoding and varied linearly in either direction.

1.3 Image-based Methods for pMRI

The first pMRI method to be used routinely was sensitivity encoding, or SENSE[11,12], in which 2D Fourier imaging with an array of receivers allows the reduction of the number of Fourier encoding steps. The reduction is achieved by sampling fewer *k*-space trajectories at increased separation, resulting in scan time reduction without the loss of spatial resolution since maximum values of *k*-space are maintained. One can characterize the acceleration in scan time by the reduction factor, R, which equals the reciprocal of the fraction of *k*-space covered during readout. Unlike standard Fourier imaging, in which individual images are acquired at a full FOV and then combined, SENSE images are acquired with the FOV reduced in the phase encoding direction (Figure 3). This FOV reduction results in aliasing. In SENSE reconstruction, a discrete Fourier transform is used to reconstruct an aliased

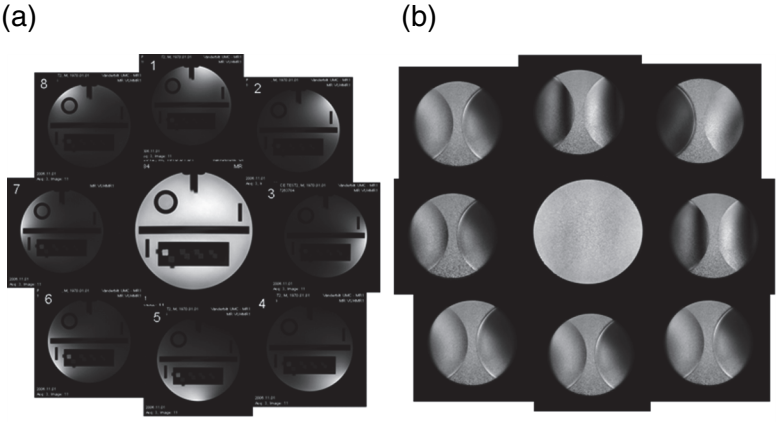

Figure 3. (a) In standard FT MR imaging, phased array surface coils acquire image data from different regions of the object being imaged, and these images are added together to form a single, uniform image. (b) In SENSE imaging with R=2, each of the datasets acquired by the coils in the array are undersampled (resulting in aliasing or wrap-around). The SENSE algorithm unwraps the image data and adds the datasets together to produce a single unaliased image acquired in a fraction of the time required to produce image (a).

image for each element in the array. Next, the full FOV image is generated from these individual sets of images. In the reduced FOV case, signal contributions from multiple locations in the full FOV are superimposed on each other due to aliasing. Hence, the second step in reconstructing a full FOV image involves separating the individual signals from underlying superimposition. Signal separation may proceed because each single-coil image signal superposition occurs with different weights according to local coil sensitivities. SENSE is known as an "image-based" pMRI method because it reconstructs images from each coil element before determining the contributions from each coil element to the image in the full FOV.

Consider n_p as the number of pixels superimposed corresponding to a number of coils given by n_c. The complex coil sensitivities at the n_p superimposed positions form an $n_c \times n_p$ sensitivity matrix, S,

$$\mathbf{S}_{\gamma,\rho} = c_\gamma(\mathbf{r}_\rho), \tag{9}$$

where the subscripts γ, ρ count the coils and the superimposed pixels, respectively, $\mathbf{r}_\rho$ denotes the position of the pixel ρ, and c_γ is the spatial sensitivity of the coil, γ. The sensitivity matrix is used to calculate the unfolding matrix, U. Using this unfolding matrix, signal separation is performed by $\mathbf{v}=\mathrm{U}a$, where the resulting vector, **v**, has length n_p and lists separated pixel values for the originally superimposed positions. By repeating this procedure for each pixel in reduced FOVs, a non-aliased full FOV image is obtained. In order to use a SENSE-based method, the sensitivity matrix must be calculated before reconstructing the final image from data gathered with SENSE.

1.4 K-space Based Methods for pMRI

SMASH (or, Simultaneous Acquisition of Spatial Harmonics[13,14]) is a partial pMRI method that relies on coil elements with variable spatial sensitivity as in the image-based methods. This variation of sensitivity with spatial position is commonly recognized with surface coils. For a standard surface coil there is an approximately monotonic fall-off of signal intensity with distance from the coil in all directions. Unlike SENSE, SMASH takes the signals' readout from each element and combines them together in differing amounts to create a composite signal. The composite signal behaves as one collected from a coil with a composite sinusoidal spatial sensitivity, by design:

$$c_{comp}(x,y) = \sum a_i c_i(x,y) = exp(-im[\gamma G_y t]y) \tag{10}$$

Here, c_i is the coil sensitivity for an individual coil, i; a_i is the weighting of that coil to create a sinusoidal composite sensitivity, c_{comp}; and m is an integer relating to the periodicity of the sensitivity. Because sets of sensitivity functions with different values of m in Equation 10 are orthogonal, one can calculate several different composite signals that sample unique information about spatial variation over the field of view. Considering Equations 8 and 10, the expression for a composite signal, S, is:

$$S(t) = \iint \rho(x,y) c_{comp}(x,y) exp(i2\pi x k_x) exp(i2\pi y k_y)\, dx\, dy \tag{11}$$

$$= \iint \rho(x,y) exp(i2\pi x k_x) exp\left(i2\pi y\left(k_y - \Delta k_y\right)\right) dx\, dy \tag{12}$$

where $\Delta k_y = m[\gamma G_y t]/2\pi$. With a particular choice of composite sensitivity, the construction of a composite signal yields spatial encoding information equivalent to phase encoding by different gradient amplitudes (in Equation 12, a shift of Δk_y has been introduced by the composite sensitivity). Hence, the modulation of a spatially varying receiver coil sensitivity function can be used to replace the phase or frequency encoding normally produced by magnetic field gradients.

In its simplest form, SMASH uses a linear array of surface coils to synthesize multiple composite sensitivity variations. The requirement for use of this linear array is that the net sensitivity of the array is designed to have a sinusoidal shape with no strict response requirements for the individual coil elements in the array. The advantage of using a coil array with multiple elements is that multiple harmonics may be generated from a single data set. The result is that a reduced number of phase-encoded lines need be acquired in a reduced acquisition time, and the remaining lines of *k*-space may be reconstructed using linear combinations of component coil signals. If a total of N spatial harmonics are generated, then N different lines of *k*-space can be reconstructed corresponding to different applications of the phase-encoding gradient. The total signal matrix can, therefore, be acquired in a fraction 1/N of the usual acquisition time.

One of the key factors in the implementation of the SMASH scheme is the determination of RF spatial sensitivities of various array elements. Uniform phantoms can be imaged since intensity variations in such images may be traced to variations in coil sensitivity. Then intensity profiles across the image plane of interest are taken from a stored phantom data set and are used as sensitivity references. The use of *in vivo* regions of comparative uniform spin density, such as in spine imaging, was also proposed. The next step in image processing is to fit these sensitivity profiles to the desired spatial harmonic function using a numerical optimization algorithm with a complex weighting factor, n_j, as the fitting parameter.

Assuming that the sensitivity information appropriate to a given image slice is known, then SMASH reconstruction involves only a set of simple weighted sums followed by matrix reordering and a discrete Fourier transformation (FT). This can be a very fast reconstruction process because individual FTs of the various component coil images in the reference algorithm are replaced in SMASH by a single FT of the combined data set.

Unfortunately, the practical implementation of SMASH is difficult. The accuracy of SMASH image reconstruction is highly influenced by the specific geometry of the phased-array receiver coil. SMASH has additional difficulty with image slices acquired in oblique orientations. Regions with relatively poor SNR create problems in synthesizing spatial harmonics. Thus, even though SMASH represents an important evolutionary step in pMRI, it has never become a standard product in commercial clinical MRI systems (Table 1).

Table 1: Acronyms of parallel imaging methods and terminology available from commercial MRI system vendors

Name	Acronym	Method	Manufacturer
SENSitivity Encoding	SENSE	Image-based reference scan	Philips
Array Spatial Sensitivity Encoding Technique	ASSET	Image-based reference scan hybrid (image- and *k*-space based)	General Electric
Auto-calibrating Reconstruction for Cartesian Imaging	ARC	Image-based reference scan hybrid (image- and *k*-space based)	General Electric
integrated Parallel Acquisition Techniques	iPAT	Used by all pMRI	Siemens
GeneRalized Auto-calibrating Partially Parallel Acquisition	GRAPPA	k-space based, auto-calibrated with reference scan option	Siemens
modified SENSitivity Encoding	mSENSE	Image-based, auto-calibrated with reference scan option	Siemens
SPEEDER	--	Image-based, reference scan	Toshiba

Currently, the most commonly employed *k*-space-based pMRI method is the generalized autocalibrating partially parallel acquisitions (GRAPPA) method. GRAPPA computes the weighting factors for constructing *k*-space lines from a few extra lines of *k*-space measured during the scan, instead of explicitly calculating coil sensitivity prior to a pMRI scan as per SENSE. Thus, GRAPPA uses the acquired *k*-space data to determine the complex coil weights required to reconstruct the image from what are known as the autocalibration signal (ACS) lines[15].

The more ACS lines used, the better the fit of the weighting coefficients, but this comes at the cost of increased scan time. Groups of lines acquired near the missing line may also be used to compute a weighted average estimate for producing the synthesized lines. Also, at high R factors, the ACS line acquisition may become a greater proportion of the total scan time. Thus the details of the scheme used for sensitivity encoding in GRAPPA may be specific to a given application as implemented by an individual software engineer.

1.5 Hybrid Methods for pMRI

The first implementations of image-based and *k*-space-based methods (e.g., SENSE and SMASH) demonstrated robust reconstruction under certain imaging assumptions. However, limitations existed—pure image-based techniques were easiest to implement but tended to produce more artifacts, while *k*-space-based methods relied more dependently on high-performance reconstruction hardware and coil design. To overcome these trade-offs, hybrid approaches to pMRI emerged. For example, the SPACE-RIP technique[16] combined the use of data in the *k*-space domain with image-based spatial measurements of coil sensitivity to reconstruct missing *k*-space data directly. This variety of pMRI relieved the dependence of SMASH-based techniques on coil design, while minimizing some of the artifact generation inherent to SENSE. Other hybrids have emerged as well[17,18].

More commonly, many current implementations of pMRI have retained their pure image-based or k-space-based methodology, but they have borrowed techniques from each other. Although auto-calibration methods are widely used in the GRAPPA method, the acquisition of ACS lines to determine an image-based calibration scan has been incorporated into image-based techniques (e.g., mSENSE). The SPEEDER implementation of an image-based pMRI technique includes a procedure named the "Extended Pi Algorithm for Unfolding" (EXPAND), which greatly reduces central artifacts that appear in image-based methods when the FOV is smaller than the tissue volume[19].

1.6 Current pMRI Methods

In summary, pMRI is a technique that allows the user to acquire images with a smaller number of excitations, which is frequently used to accelerate an MRI acquisition. To accomplish this, a number of phase-encoding steps are replaced with spatial encoding that arises from the spatial sensitivity of multiple receiver coil elements at particular locations. As a result, all pMRI techniques rely on direct (calibration scan) or indirect (autocalibration) determination of the spatial sensitivity for each coil element, before or during a scan. The reduction or acceleration factor, R, characterizes the reduction in the number of phase-encoding steps executed by the scan. Some MRI systems require that R is an integer, while other vendors allow non-integer R values. Current pMRI techniques fall into the two techniques, or hybrids blending the two (see Table 1). Image-based techniques (e.g., SENSE) take undersampled data from each coil element and reconstruct individual aliased images before unfolding the data into the full image with a matrix. The *k*-space based techniques (e.g., SMASH, GRAPPA) first create a full dataset using the partially sampled *k*-space data from each coil element before performing an inverse Fourier transform to compute the full image.

2. Clinical Applications for Parallel MRI

2.1 General Uses of Parallel MRI

The most common clinical application of pMRI is to reduce the time required to acquire the MR image data. It is especially useful in body imaging since motion from breathing and peristalsis can often compromise image quality. In the body, the greater imaging efficiency derived from pMRI can also be used to improve spatial resolution in the same total scan time by increasing the number of phase-encoding steps. This approach assumes that there is adequate SNR available. The use of pMRI is particularly beneficial for higher field-strength scanners (≥3T) because it allows multiple ways in which to use the additional SNR available while reducing the number of RF pulses required per TR, thus reducing specific absorption rate (SAR) of a study.

Parallel imaging has sweeping importance precisely because it is flexible and can be combined with virtually any type of pulse sequence. For example, one may combine parallel imaging with other fast imaging methods (EPI, FSE) in order to achieve "real-time" image acquisition, of particular interest in interventional MRI. Many applications for pMRI in a range of clinical areas have become standard practice. Some of the benefits achieved and the problems encountered are described below.

2.2 Balanced Steady-state Gradient-echo Imaging with pMRI

It is generally assumed that the use of pMRI to achieve either greater imaging speed or improved spatial resolution will also result in reduced image SNR. However, Weiger et al.[20] have demonstrated that pMRI can be used to enhance image SNR under certain circumstances, especially when using fast gradient echo imaging methods for contrast-enhanced MR angiography (CE-MRA). Increases in SNR can be gained using pMRI in steady-state gradient echo sequences in which longer TR or reduced receiver bandwidth would lead to increased signal. This has been confirmed by deVries, et al.[21] who reported that SNR and CNR were improved using SENSE imaging in CE-MRA studies in peripheral vessels. CE-MRA can also exploit the increased imaging speed of pMRI to reduce venous contamination in regions having rapid venous return, such as renal and carotid arteries.

2.3 Spin-echo Trains for T2-weighted pMRI

At field strengths of 1.5T and higher, T2-weighted MR images are generally obtained using spin-echo methods, in which multiple echoes are used to obtain multiple discrete *k*-space lines in the phase-encoding direction. These methods are variously known as fast spin-echo (FSE), turbo spin-echo, FIESTA, or HASTE. However, these methods suffer from two limitations. First, the amount of time required for the echo train to play out limits the number of slices that can be obtained within the conventional TR time frame used in T2-weighted imaging. Second, the extended acquisition of multiple spin-echoes with FSE sequences takes a time that is greater than the T2 of most tissues, causing the signal amplitude for these tissues to be reduced by different amounts between adjacent phase-encoded lines. The result is a T2-dependent blurring of the image in the phase-encoding direction.

Parallel MRI with FSE can be used to reduce the echo train length by the pMRI reduction factor, R which, in turn, allows scans to have more slices with a given TR. One can also use pMRI with FSE acquisitions to reduce the time for the echo-train to be acquired, minimizing T2-dependent blurring (see Figure 4) and preserve spatial resolution that would otherwise be lost during the long effective-TE. Parallel MRI is beneficial when used with FSE-type breath-hold acquisitions that employ reduced *k*-space acquisitions. Finally, pMRI also allows modification of signal averaging strategies for motion artifact reduction in abdominal imaging[22,23].

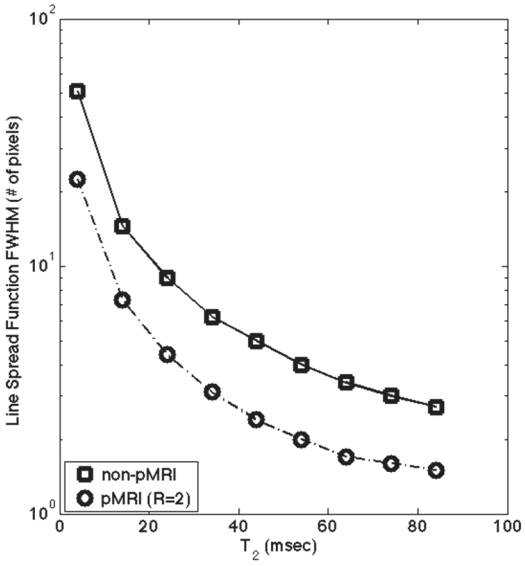

Figure 4. FWHM of the line spread function versus T2 in a turbo Spin Echo acquisition demonstrates resolution improvement available using SENSE vs. conventional imaging. In this case the SENSE image with R=2, required an echo train length (ETL) of 48 while for conventional imaging ETL = 96. Adapted from reference 24.

2.4 Dynamic Parallel MRI

Dynamic imaging is the successive acquisition of images from the same tissue volume for the purpose of following the time course of physiological events. Typical goals of dynamic MRI are to acquire images of an object in motion (e.g., cardiac function) or to follow a contrast agent as it makes its way through the body (e.g., perfusion imaging). Unfortunately, limitations in gradient performance and physiological constraints (e.g., peripheral nerve stimulation) restrict image acquisition speeds gained exclusively from faster gradient pulsing. Since pMRI can produce images without having to fill the full *k*-space volume at each acquisition time, imaging speed can be increased without changing gradient performance.

Cardiac imaging has been greatly enhanced by pMRI. In cine sequences for evaluating cardiac function, pMRI can reduce the required number of cardiac triggers, significantly diminishing the artifacts due to missed triggers or reduce the length of a breath-hold. The clinical use of dynamic contrast enhanced (DCE) imaging of the breasts, heart, and prostate is rapidly becoming routine. Parallel MR imaging allows increased spatial coverage of the heart or the breast without increasing the acquisition time so that the uptake curves can be displayed with sufficient temporal resolution to distinguish normal from pathological enhancement patterns.

In addition, pMRI concepts can be extended to further reduce the number of lines acquired per image by taking advantage of information obtained from the same volume of tissue at various times. Unlike standard protocols that acquire images covering one volume during acquisition, dynamic imaging acquires many images throughout time. Correspondingly, the standard protocol acquires data within a volume of *k*-space to assemble the spatial image, whereas dynamic imaging protocols acquire data within both *k*-space and *t*-space to assemble many images over time. With the standard pMRI, data acquisition is accelerated by collecting only a fraction of *k*-space and reconstructing the missing data. Parallel MRI is one technique that follows this approach, but another common technique is partial Fourier acquisition. The partial Fourier reconstruction is possible because information about missing *k*-space data is retained in the fraction of the acquired *k*-space data; in other words, spatial

correlations exist in the data. In the case of partial Fourier techniques, redundancy in *k*-space itself allows the full space to be reconstructed from a smaller, selected sample. Parallel MRI strategies take advantage of the correlations that arise from sampling a region with multiple coil elements.

One difference between standard pMRI and pMRI in dynamic acquisitions is that data can be undersampled in both *k*-space and in time. Dynamic pMRI is used to examine changes within a region over time. Because the expected change is small or negligible in certain parts of the image over time, a dynamic image series possesses some degree of spatio-temporal correlation. The domain of these spatio-temporal correlations is often called *k-t* space, and one can perform an equivalent technique to pMRI by collecting a fraction of data within *k-t* space. Using this approach, the data comprising each image in the dynamic protocol is undersampled in *k*-space, and this sampling pattern is altered as time progresses. To reconstruct the missing data, data sampled at different places in *k*-space and at different times are used.

Reducing scan time in dynamic imaging by taking advantage of temporal correlations does not require pMRI. A dynamic imaging strategy, dubbed UNFOLD, alternately samples even and odd lines in *k*-space over time and zero-fills the rest[25]. Dynamic pMRI adopts approaches similar to UNFOLD and incorporates them into the pMRI scheme. For example, the temporal SENSE (TSENSE) method combines image-based pMRI with UNFOLD[26]. If only one image was acquired, the missing lines would result in an aliased image. The application of a 4D Fourier transform converts *k-t* space to *x-f* space. The undersampling results in a frequency shift of aliased components. Filtering in the frequency domain removes the aliased components before a final transform produces spatial images over time. The alternate sampling of lines as time progresses represents a specific, restricted sampling scheme in *k-t* space. Another method, *k-t* SENSE, relaxes this constraint to allow for general patterns of data undersampling throughout *k-t* space[27]. Finally, the *k*-space-based dynamic pMRI analog to this technique is named *k-t* GRAPPA[28]. One advantage of undersampling the data in *k*- and *t*-space is that higher pMRI reduction/acceleration factors than standard pMRI may be possible while retaining good SNR. Important areas of application for dynamic parallel imaging with temporal undersampling include BOLD contrast fMRI and phase-contrast MR flow imaging[29].

2.5 pMRI in T2*-weighted imaging

Parallel MRI may be used to achieve higher imaging rates for dynamic susceptibility-weighted (T2*) echo-planar imaging (EPI). However, extreme reduction of TR can cause the images to be less T2*-weighted and somewhat contaminated with T1 weighting. A dual-echo approach has been used to mitigate this problem and also to avoid signal saturation effects in large vessels during bolus passage of the contrast agent. Instead of using pMRI for achieving a higher imaging frame rate, one can capitalize on the shortened EPI readout to collect more imaging slices for improved tissue coverage.

In general, EPI is vulnerable to local susceptibility gradients that disturb the spatial fidelity of structures in the image. Artifacts that can occur include intravoxel dephasing of the NMR signal, which is a shifting of the signal so that there are regions of increased and decreased signal intensity in the region of the susceptibility gradient and geometric distortion (Figure 5). These EPI artifacts occur in the phase-encoding direction, even though in conventional FT-MRI they are prominent in the frequency-encoding direction. These artifacts arise from the accrual of phase errors during the course of signal acquisition. Interleaved EPI methods (multi-shot EPI) have been shown to be effective in reducing these artifacts; however, the extra time required for multiple RF excitations limits the clinical utility of multi-shot methods for applications such as diffusion imaging and contrast-enhanced susceptibility weighted imaging in the brain. The use of pMRI methods with functional brain imaging can reduce the number of echoes acquired and, therefore, reduce the accrual of phase errors. In addition, a reduction in the effective TE of the echo train may be possible, which can mitigate losses of

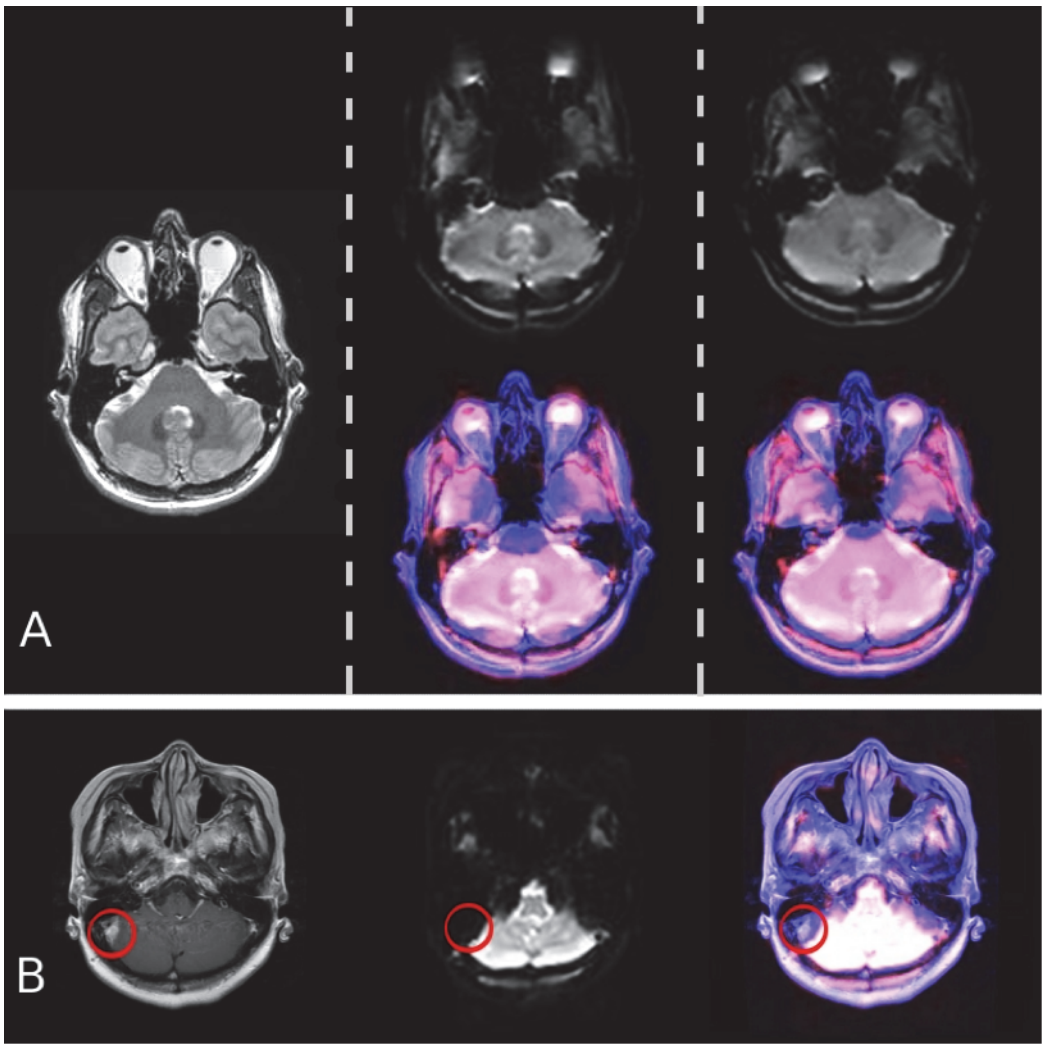

Figure 5. Clinical use of pMRI with EPI sequence. Panel A: Left frame shows a T2W anatomical image for reference. Middle and right frames show EPI images (top) for no pMRI (middle) and pMRI with an acceleration factor of two. Bottom images in the middle and right frames show the EPI images in red as an overlay to the T2W anatomical image in blue. Note that regions of susceptibility result in more registration error for the EPI image without pMRI. Panel B: T1W post-contrast image of patient with enhancing cerebellular lesion (red circle) is shown in the left image. EPI-based dynamic susceptibility imaging for perfusion (middle image) without pMRI eliminated the lesion from the image, as shown in the right image overlay.

SNR at increased R values. One may also use the decreased image acquisition time to increase the b-factor of the diffusion-weighting gradient without an additional SNR penalty. Finally, pMRI can also reduce the appearance of artifacts due to changes in tissue susceptibility that occur when contrast agents make their first pass through the tissue in a tight bolus.

2.6 Adapting Clinical Protocols to pMRI

As mentioned in previous sections, the increased flexibility afforded by pMRI offers a variety of benefits—reduced scan time, increased spatial resolution; increased SNR, and reduced artifacts. However,

not all benefits are useful in every clinical circumstance. Furthermore, possible tradeoffs to these benefits—decreased SNR and the introduction of new artifacts—may be acceptable in some protocols, yet detrimental in others. Thus each pulse sequence within a standard protocol should be evaluated to determine how it may benefit from some application of parallel imaging principles within the context of the overall study. Augustin et al.[24] have discussed a stroke imaging protocol in which pMRI is used to increase temporal resolution in dynamic susceptibility-weighted contrast studies of brain perfusion and time-resolved contrast-enhanced MRA, improve spatial resolution with minimal signal loss in T2-weighted fast spin echo, and reduce geometric distortion in diffusion-weighted imaging with the echo-planar (EPI) method. Chung and Muthupillai[30] have described how SENSE can be used to benefit pediatric body MRI studies. Similar considerations will apply to heart, liver, and breast studies, among others.

3. Radio Frequency Coils in Parallel Arrays

3.1 Surface Coils and Phased-array Coils in Clinical Use

Surface coils are radio frequency (RF) coils that were originally used for *in-vivo* MR spectroscopy studies to improve sensitivity. These coils operated in transmit–receive mode so that the complication of nonuniform excitation, as well as nonuniform signal reception, existed. Using these coils, spectra with signals from low-concentration metabolites could be obtained from superficial living tissues.

In 1984, Axel and Hayes proposed the use of surface coils to improve sensitivity in clinical MRI studies[31]. Surface coils produce signal-to-noise ratio (SNR) improvements in two ways. First, the signal is increased by the coils being closely coupled to the volume of tissue under investigation. Second, the noise is decreased because the surface coils do not receive thermal noise from parts of the patient's body that are not being imaged. The surface coils of Axel and Hayes were receive-only; the integrated, body RF coil was used for transmitting the RF pulses. Simple, linear surface coils consist of one or more conductive loops; whatever the physical arrangement, the signal is received on a single RF channel. This configuration improves the SNR of the typical clinical MRI study by a factor of 5–10 in regions near the coil. However, the nonuniformity in the images generated by simple surface coils is often considered objectionable, and geometrical placement of the coils is of critical concern. Additionally, the tissue interrogation depth is limited by the relatively small coil diameter. To overcome this problem, methods for correcting the MRI intensity have been proposed, but these tend to produce images that have variable graininess[32].

In 1986, Hyde et al. proposed the use of multiple receiver coils arranged in phased-arrays to maintain the advantages of surface coils while extending the depth of investigation and improving the overall uniformity of the images they produced[33]. These coils have become standard equipment used for most MR imaging in the torso, abdomen, pelvis, and extremities.

Unlike simple surface coils, a phased-array RF "coil" consists of multiple surface coils, operating as separate elements on independent RF channels. The signals from the coils are combined after digitization. Assuming a two coil-element array, SNR increases up to $\sqrt{2}\times$ increase can result if the noise signal received by the elements is uncorrelated, for example. To achieve this result, a switching circuit must be employed to ensure that the RF transmitter coil and the phased-array receiver coil do not interfere with each other. The most common active element of these switches is the PIN diode[34]. PIN diodes contribute low insertion loss in the forward bias state, which is important since many diodes are used for each array, and the combined losses must not be significant. Also, in the reverse bias state, PIN diodes have very low leakage currents so that the isolation between the transmitter and the receiver channels is maintained with little noise added. It is also important to note that special PIN diodes with non-magnetic packaging must be used for magnetic resonance applications[35].

3.2 The g-factor and SNR in pMRI

Parallel imaging requires the use of phased-array coils to replace part of the spatial-encoding process via phase-encode gradients with spatial localization via the positioning and sensitivity of coil elements. Phased-array coils used for pMRI work optimally when the signals (both NMR signal and noise signal) recorded through the multiple RF channels are uncorrelated. To achieve this goal, the coil elements and associated electronics are designed so that the mutual inductive coupling is minimal. Inductive decoupling of coil elements may be achieved by several strategies (see Kwiat et al.[8] and articles cited therein). Most simply, the coils can be arranged geometrically so that the magnet flux lines from one do not intersect the plane of another. However, this passive solution becomes more difficult to achieve as the number of coil elements in the array increases. Additionally, the transformation methods used in the coil-encoded parallel MRI methods are different from those used in traditional Fourier imaging in that they are not commonly unitary, i.e. their inverse is not equal to their complex conjugate. Because of this, an additional, spatially dependent source of noise exists in parallel imaging with coil arrays.

The signal-to-noise ratio (SNR) for pMRI is related to the SNR in traditional Fourier imaging by the following relationship:

$$SNR_{pMRI} = \frac{SNR_{fullacquisition}}{g\sqrt{R}} \tag{13}$$

where R is the pMRI acceleration factor (R=1 implies a full acquisition, R>1 implies an image acquisition acceleration factor). The local geometry factor (g-factor) of the coil array is used as an index of the geometry-related SNR loss obtained in parallel imaging. Any further SNR degradation in pMRI is attributed to the mathematics of reconstruction. By definition, g is theoretically expected to always be greater or equal to one. From this theory one would not expect the parallel image reconstruction process to improve SNR (g<1).

Practically, the *g*-factor is an important criterion for modeling the design of coil arrays[12,36]. The unfolding process can amplify the noise found in the aliased pixel as it distributes the signal and noise to the multiple unaliased locations. For example, consider a two-element receive coil and an image where two pixels are aliased together. A two-equations (two elements), two-unknowns (two spatial locations; coil element sensitivities at both locations are known) set of equations will describe how the individual pixels are aliased together. If the two equations are identical, the two individual pixel intensities cannot be computed. The equations (elements) are never identical in practice, but the more similar the equations, the greater the amplification of the aliased pixel noise when split into the individual unaliased pixels, even if the spatial coil element sensitivity maps are perfect. Since the equations are different at each aliased pixel location, the image noise is different in each pixel. It should be noted that *g*-factor improvements can be realized by excluding pixels from known noise-only regions. Thus, it is possible to mask out noise-only regions in the final image. This has implications for measuring noise in background, noise-only regions.

The *g*-factor is used to describe the ability to unwrap a particular aliasing pattern, given a specific coil geometry. As such, *g* is influenced by coil placement with respect to the region of aliased anatomy (i.e., slice position, orientation, and phase-encoding direction) as well as coil decoupling. The *g* factor tends to be smallest near the coils, where contributions from individual coils are easily separated, and larger away from the coils, where signal contributions to a pixel from individual coils may be difficult to assess and the unwrapping algorithms result in larger uncertainty in the unwrapped signal.

Recent investigations aimed at determining the maximum SNR that may be available using parallel MR imaging under a variety of imaging conditions suggest that coil sensitivity functions are more

readily manipulated with more coil elements and at higher magnetic field strengths in general. More specifically, Ohlinger et al. have examined the case of the pMRI study in which the patient to be imaged is the major source of noise signal[37]. These investigators show that in this case any loss in the sensitivity of the study may be compensated by using information gained from measuring the coil correlations.

3.3 Phased-array RF Technology for pMRI

The *g*-factor itself has a dependence on *R*, where *g* increases with increasing *R*. SNR decreases with increasing *R*; however the rate of SNR decreasing with *R* can be slowed by designing more elements into the pMRI coil[37], as illustrated in Figure 6. Unfortunately, the gains in SNR with increasing numbers of coil elements produces diminishing returns, at least at resonant frequencies below 100 MHz. In principle, a well-designed coil with many elements can lead to greater acceleration factors. One question currently under investigation is, "What is the optimal number of data channels for a particular application of parallel imaging?" Certainly, increases in the amount of cabling and electronics will increase the amount of noise per image, which might require cooling or the use of wireless communication[38].

Preliminary studies indicate that images with clinical utility can be produced using higher numbers of channels and larger acceleration factors than are typical in basic pMRI clinical systems (8 channels, acceleration ~2). Premium systems offer more RF channels, and multiple research sites have reported results using 32-channel systems[36,38], choosing acceleration factors of 7–16 and producing images of reasonable quality. More exotic systems include a 96-channel system with 23- and 90-element head coils[40]; and a 4.7T system[41] equipped with a 64-channel planar RF coil that has demonstrated an acceleration factor of 64, although the image is of low quality. Two vendors (Toshiba and Siemens) currently offer scanners with 128-receiver channel capability, although individual coil arrays generally have significantly fewer channels. Tradeoffs between clinical benefits and speed gains using large numbers of channels depend largely on the application being considered. Most designers of modern commercial MRI systems have adopted a scalable, modular design for their RF systems so that it may accommodate whichever number of coils elements is determined to be desired for a given study at any field strength. One vendor (Philips) has opted for incorporating ADCs into each coil element, so that only digital fiber optic signals go to the image processing computer.

If we currently cannot answer the question of how many channels are optimal, we have learned that depth sensitivity at smaller element size is not a fundamental limitation.

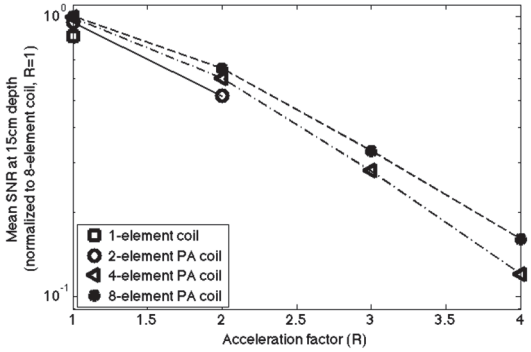

Figure 6. Diagram illustrates how the reduction in SNR with increasing acceleration factor (R) is less in array coils with more elements. Adapted from reference 38.

Sodickson et al. predicted that sensitivity of the whole array to depth does not limit SNR as the element sizes shrink, and data collected with arrays having different numbers of elements agree with these simulations[38]. Data also indicate that SNR at larger depths may be affected at low acceleration rates for increased numbers of elements. This suggests that coils with large numbers of elements may be used only for clinical exams requiring very rapid image acquisition speeds, while phased arrays with smaller numbers of elements would be used for other standard applications.

4. Reconstruction Artifacts in pMRI

Parallel MRI techniques are unique in that they are designed to generate a specific artifact on the acquisition side, namely aliasing in the image domain from the under-sampling of *k*-space. The success of the entire process depends on the ability to remove this aliasing artifact without compromising the diagnostic integrity of the resulting images. Under the primary assumptions that the individual coils in the array provide enough unique spatial information and that the coil sensitivity information is known, pMRI reconstruction can remove this aliasing artifact successfully with minimal detriment to the overall quality of the image.

Unfortunately, these assumptions can be violated due to a host of issues, each leading to different varieties and magnitudes of artifacts in the resulting image. Adding an extra level of complexity, the development and evolution of new pMRI technology may render current artifacts relatively non-existent in the future, while new types of artifacts may emerge. Generally, the primary sources of these violations include incorrect estimation of the coil sensitivity, limitation of the pMRI reconstruction methodology, and hardware limitations. Because reconstruction methods rely heavily on matrix inversions or bounded fitting routines, small errors in the coil sensitivity or *k*-space trajectory can lead to large errors in the reconstructed image. In all cases, the primary artifacts associated with pMRI tend to be residual aliasing in the image, or inconsistencies introduced into the image by the reconstruction process. Image-based pMRI techniques, such as SENSE, are susceptible to different types of artifacts compared to *k*-space driven techniques, such as GRAPPA. Additionally, the use of autocalibration techniques may alleviate some artifacts associated with pre-scan calibration techniques, often for a minor sacrifice of imaging speed.

4.1 Hardware-related Artifacts

As demonstrated in Equation 8, the reconstructed image SNR is dependent on both the acceleration factor (R) and the geometry factor (g). The g-factor varies over the image, being smaller in close proximity to the coils. This results in spatially varying degrees of noise and artifacts in pMRI which tend to be more severe at the center of the image and with increasing R factors (Figure 7).

Because of this, the positioning of coils on the patient as intended by the manufacturer is crucial to successful pMRI. Often, arrays designed for breast, body, or spine imaging have a preferred direction of sensitivity. Choosing to employ phase-encoding in a direction with a high g-factor can result in poor image quality and aliasing artifacts, particularly at $R>2$. If a coil has a preferred orientation of spatial sensitivity, the direction of phase-encoding should always match the intended direction as indicated by the coil manufacturer.

Additionally, hardware issues that result in inconsistent signal quality (e.g., failed coil element, receiver saturation, poor field homogeneity, or gradient nonlinearities across the volume of interest) can also lead to artifacts due to the introduction of discrepancies between the acquired image and coil

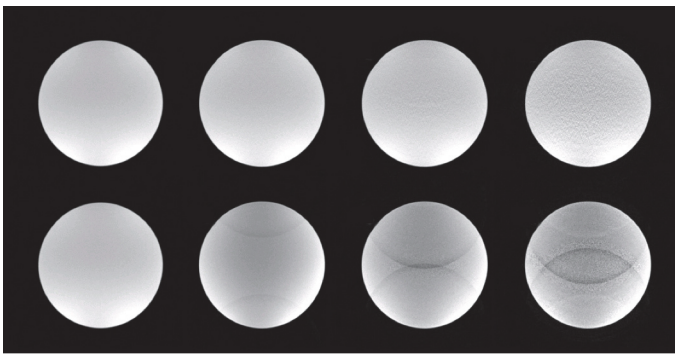

Figure 7. Artifacts in GRAPPA (top row) versus mSENSE (bottom row) as a function of acceleration factors (column) with a fixed number of integrated oversampling *k*-space lines (n=24) in a homogeneous phantom at 1.5T using turbo spin echo (TR/TE=300 ms/8.6 ms; matrix = 256 x 256; FOV = 240 x 240; rBW = 260 Hz/pixel; echo-train length = 3) in a standard phased-array head coil.

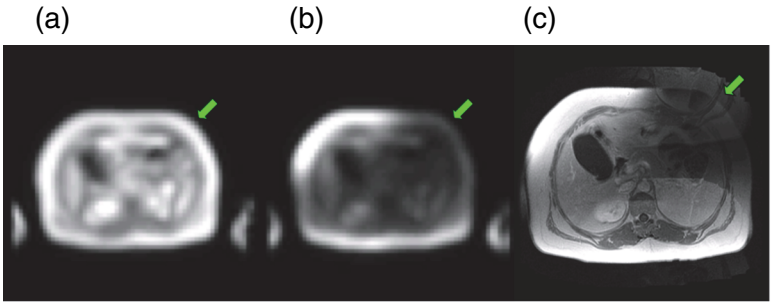

Figure 8. Coil geometry plays an important role in pMRI. When a coil element fails or returns spurious signal, the loss of information is propagated as an artifact. Above the calibration scan from the body coil (a) compared with the calibration scan from the array (b) show signal fall-out of one of the elements, which results in artifacts (c).

calibration (Figure 8). In the case of failing coil elements or poor field homogeneity effects, using autocalibrated sequences may be worth the loss in temporal resolution to temper these artifacts. In cases of sharply changing signal intensities or gradient inhomogeneities warping the anatomy, autocalibrated *k*-space methods may confer an advantage over image-based approaches since they can incorporate the coil sensitivity information in *k*-space and avoid problems with aliased or rapidly changing coil sensitivity maps in image-space[42,43].

In the case of high-speed (i.e., EPI) or non-Cartesian *k*-space acquisitions, errors in the trajectory itself (such as those associated with eddy currents, gradient nonlinearity or concomitant field terms) can also lead to significant problems, as this can cause an incongruence between the image and the acquired calibration map. In this scenario, *k*-space-based methods are likely a better choice as they are better suited for handling artifacts associated with geometric distortions. For EPI based applications, such as fMRI[44] or diffusion imaging[45,46], k-space techniques consistently result in less image artifacts than their image-based counterparts.

4.2 Field of View Artifacts

Often the field of view (FOV) selection in MRI tightly constrains the imaged tissue volume in order to obtain the highest possible resolution in the minimum amount of time. In non-pMRI protocols like oblique cardiac imaging, wrap-around artifact in the periphery of the field of view is tolerated in order

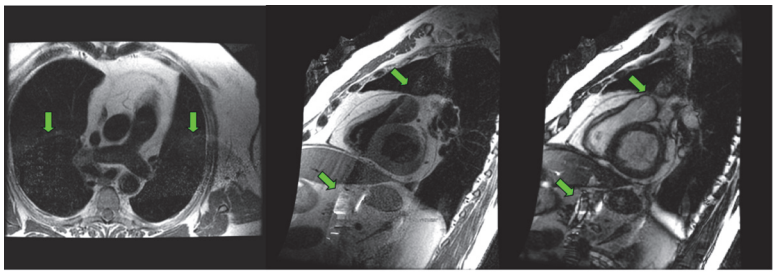

Figure 9. Image-based parallel imaging techniques that rely on a coil sensitivity map (e.g., SENSE) assume that the anatomy has been aliased only once. If a field of view is selected which is smaller than or too close to the extent of the anatomy of interest, parallel imaging acquisitions alias the anatomy twice and result in artifacts. *K*-space pMRI techniques, such as GRAPPA, do not have this problem, making them useful for acquisitions that require reduced fields of view, such as oblique views in cardiac imaging.

to achieve higher spatiotemporal resolution, as long as the aliasing doesn't interfere with the region of interest. Because pMRI techniques further reduce the FOV by the acceleration factor, aliasing in the periphery can present additional problems for image-based pMRI techniques, as they rely on unfolding a matrix in image space[42]. This scenario introduces large signal artifacts or noise from the peripheral aliasing into the center of the image (Figure 9). However, just as with the geometric distortions described earlier, *k*-space techniques do not suffer from this limitation and are, therefore, a better choice when the full FOV image contains aliased information[43]. So, with image-based techniques, a FOV of proper size must always be prescribed slightly larger to accommodate geometric distortions that might place the anatomy outside the FOV and cause additional aliasing. A *k*-space technique should be considered if either one of these conditions cannot be met.

4.3 Coil Calibration-based Artifacts

Residual aliasing occurs when the calibration scan and the pMRI scan are not in concordance with each other. The calculated coil sensitivity maps used to unwrap the images must provide accurate representations of the sensitivities at the time the image was generated. The most common method for acquiring coil sensitivity information is to execute a calibration scan across the region of interest prior to the pMRI acquisition. This fast, low-resolution calibration scan can be used to calculate the coil sensitivities, which are assumed to be slowly varying or static.

There are numerous points at which the separate calibration scan can fail. First, if a substantial portion of the calibration scan volume doesn't include signal from the anatomy during the calibration part of the scan, the coil sensitivity map cannot be calculated. Anatomy that moves into this area during the pMRI acquisition won't appear in the image, and a signal void will be present (Figure 10). This also means that signal ghosts (motion, flow, etc.) outside the calibration scan volume will be suppressed.

If, conversely, there is signal in the calibration scan that doesn't belong, such as motion or flow ghosting, the coil sensitivity in that area will be in error and image artifacts will likely result. Outside the anatomy, this situation can result in streaking artifacts from the incorrect coil weighting and ill-conditioned inversion matrix. Inside the anatomy, this results in improper coil sensitivity maps and residual aliasing artifact. At high acceleration factors, even auto-calibrated sequences may experience this problem.

Another consideration with respect to motion is that only a slight misregistration in the region near the surface coils—where the signal intensity gradient can be very high from adipose tissue and the close proximity of the coil—can result in significant residual aliasing artifacts (Figure 11).

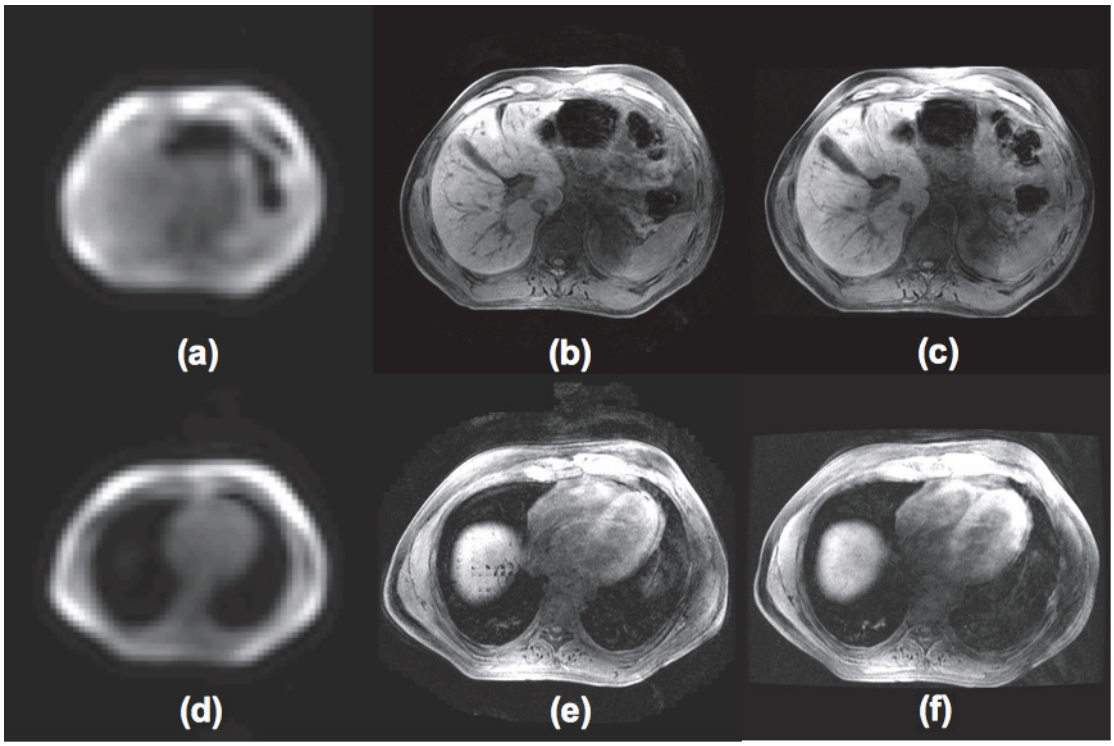

Figure 10. A 3D gradient echo based exam in the liver uses a breathold calibration scan (a) and (d) for SENSE reconstruction in the center of the liver (b) and the dome of the liver (e). Note that the corresponding slice of the calibration scan (10 mm thick slices; 32 x 32 matrix; 48 x 48 cm FOV) in (d) does not show the dome of the liver and instead presents a signal void. The coil sensitivity function is not fully interpolated into this region, resulting in artifacts in (e). A 30% reduced phase field of view acquisition (c and f) achieves similar SNR, has no parallel imaging artifacts, but can cost more time for the same coverage and resolution.

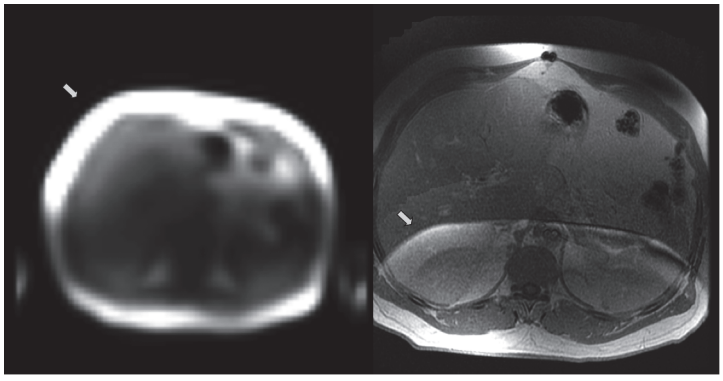

Figure 11. The large signal gradient in the near field of the coil, such as caused by subcutaneous fat changes, results in large residual aliasing artifact. These artifacts can be reduced by using a standoff pad between the patient and coil.

The practical remedies to the coil calibration problems are to 1) ensure that the calibration scan is centered on the volume of interest, 2) ensure that the coverage includes all anatomy in the range of the sensitivity of the coil that can potentially be aliased into the image, and 3) ensure that the image ghosts are kept to a minimum by using breath holding techniques if necessary. Using a standoff pad to distance the coils from the patient's skin can also significantly reduce residual aliasing. However, the approach of tightly registering the calibration scan and acquired images is prone to failure in regions where there is substantial motion (i.e., the heart or abdomen) or extended scan times are to be used, such as for dynamic imaging. For these cases, the slight time penalty associated with adding a few lines of *k*-space via auto-calibration is likely to be worth the increased resistance to artifacts. Additionally, for auto-calibrated sequences, the extra lines of *k*-space now contribute directly to the image signal as well, boosting the SNR.

Of course, the primary drawback to auto-calibrated techniques is the loss of the advantages that came with the reduced *k*-space acquisition. For Cartesian techniques, the primary penalty is slower imaging speeds; for EPI, the resultant image quality is degraded due to a reduced echo-train that results in decreased distortions and T2* blurring effects. For EPI acquisitions—where motion can be mitigated more easily, such as neuroimaging—a wiser choice may be to avoid auto-calibration. However, if significant field drift occurs during scanning, as per fMRI acquisitions, the use of a calibration scan could still result in residual aliasing artifacts. To this end, view-sharing acquisition techniques that dynamically embed the auto-calibrating parameters in the MRI acquisitions over time are becoming more widespread. These methods provide balance between fast dynamic and EPI-based applications without the need to add extra lines of *k*-space.

Table 2 organizes the discussion in this chapter by artifact type, pMRI flavor, and potential solutions for a given artifact. In this manner, Table 2 may serve as a quick reference guide for diagnosing particular pMRI artifacts and for recommending changes in protocol for better image quality.

Table 2: Parallel imaging artifacts—major causes and solutions

ARTIFACT (major cause)	PPI S	PPI G	PPI A	POTENTIAL SOLUTION
RESIDUAL ALIASING				
high coil *g*-factor	+	+	+	alternative PE direction; reduce R; coil selection
higher order aliasing (small FOV)	+	–	±	increase FOV; reduce R; alternate PPI technique
higher order aliasing (distortion)	+	–	±	increase FOV; reduce R; alternate PPI technique
coil sensitivity error (motion)	+	+	–	breath-hold; alternate PPI technique
coil sensitivity error (coil element)	+	+	–	repair coil; alternate PE direction; reduce R; alternate PPI
coil sensitivity error (B_0/B_1)	+	+	–	system PM/repair; reduce coverage; alternate PPI
coil sensitivity error (grad. dist.)	+	+	–	system PM/repair; reduce coverage; alternate PPI
coil sensitivity error (high intensity)	+	+	–	system PM/repair; reduce coverage; alternate PPI
BLOCKING (INTERPOLATION ERRORS)				
motion of anatomy near signal void	+	+	–	breath-hold; alternate PPI technique
signal loss (B_0/B_1)	+	+	–	system PM/repair; reduce coverage; alternate PPI
MISSING ANATOMY				
anatomy not covered in cal scan	+	+	–	new calibration scan; alternative PPI technique
coil elements not used in cal scan	+	+	–	new calibration scan; alternative PPI technique

S=SENSE-like PPI technique; G=GRAPPA-like PPI technique; A=Auto/self calibrating PPI technique (SENSE/GRAPPA)

5. Measurement of Image Quality in pMRI

5.1 Measuring the Signal-to-Noise Ratio in pMRI

The SNR is an important determinant of image quality. SNR is typically measured using a relatively large region of interest (ROI) and sampling a large number of pixels to minimize the effect of pixel-to-pixel variation on the measurement. As pMRI techniques accelerate image acquisition by sub-sampling *k*-space in the phase encoding direction(s), resolution is unchanged at the expense of image SNR. Unfortunately, these specially reconstructed images have spatially varying noise characteristics that violate the assumptions underlying typical large ROI SNR measurements. Therefore, it is useful to understand the SNR characteristics of pMRI and how to measure the SNR properly. Understanding the spatial variation in image SNR can help guide pMRI parameter selection and optimize pMRI coil design.

Symmetrically sampled *k*-space MR data sets typically are assumed to have white, zero-mean, Gaussian distributed noise and produce images with spatially constant noise. The mathematical term for this condition is "ergodicity."

In the case of a typical magnitude FT image reconstruction, the magnitude operation rectifies the complex image domain, zero-mean, Gaussian distributed noise into a real, positive value only, asymmetric Rician distribution with a non-zero positive mean[47,48].

For a given sequence and image resolution, the received signal is constant, but image domain noise changes by the acquired number of *k*-space data points. This results in the well-known relationship:

$$SNR \propto \sqrt{n} \tag{14}$$

where n indicates the number of *k*-space data points acquired. Since pMRI methods collect fewer data points, SNR is always lower than the fully acquired, otherwise equivalent acquisition.

The noise characteristics of pMRI are further complicated by the variation of spatial sensitivity for each individual coil element, by the particular algorithm chosen for image reconstruction, and by the inevitable interaction of elements within a coil. While the coil elements have unique spatial sensitivities, various coil elements can share noise simultaneously. The degree of noise interaction between coil elements can be mathematically characterized by a noise correlation matrix, Ψ[49], which contributes to the g-factor.

Since the reconstruction mechanisms for image-based and *k*-space-based forms of pMRI are fundamentally different, it is necessary to consider their impact on image noise separately. While the theoretical details of noise in pMRI images may vary as a function of the pMRI reconstruction algorithm used, all algorithms produce images with spatially variant noise characteristics. Additionally, other proprietary details, such as masking and thresholding algorithms, may exist in the various manufacturers' reconstruction processes. Presently, there is no complete theoretical SNR analysis of all *k*-spaced based methods similar to the g-factor theory. Therefore, a qualitative description of some interesting noise properties is provided, illustrating aspects of spatial noise variation in *k*-space-based pMRI methods.

It is assumed that the typical MR image uses fully and symmetrically collected *k*-space with an equal number of averages per phase encode line. Consider the situation where the numbers of averages per phase encode line are not constant through all of *k*-space. As the number of averages for the middle region of *k*-space is increased, the SNR is improved for those lines only. Because the middle of *k*-space is responsible for lower spatial frequencies, the noise in a reconstructed image will not be distributed equally at all spatial frequencies. As a result, the image noise has a different texture[50]. While

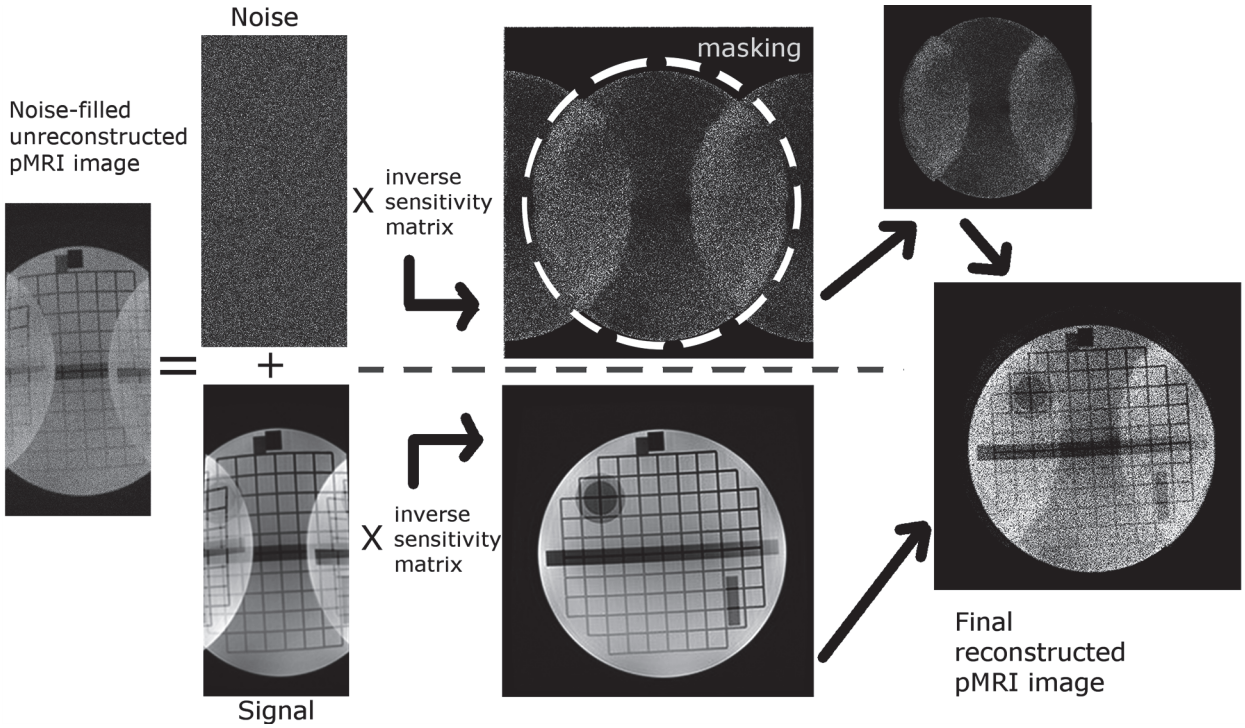

Figure 12. Simple diagram illustrates how the pMRI signal and noise are treated separately in the SENSE reconstruction process as the algorithm moves from the beginning (left side of diagram) to the end. For demonstration purposes, the contribution from noise is exaggerated for clear visual identification. Adapted from reference 50.

the texture is different, there is no spatial dependency. However, a short-range spatial correlation has now been introduced by the variable weighting in *k*-space. This short-range correlation may have consequences in the experimental measurement of SNR in pMRI methods, depending on the measurement method. For example, if noise is correlated over a short range, small ROI noise statistics measurements may not be accurate.

Now consider a single-channel *k*-space data set that has been under-sampled by a factor of two. The *k*-space pMRI methods fill in the missing lines by interpolation using multiple channels, and the interpolation effectively restores the full FOV. The noise in the collected data lines is ideally random, but the noise in the interpolated lines is a weighted average of the noise in the collected lines. The averaging process also lowers the noise amplitude. The noise in the outer regions of the full FOV will have different amplitude and texture compared to the noise in the middle regions of the FOV (Figure 12). Changing the acquisition acceleration factor changes the amplitude and texture between both regions.

In practice, *k*-space based parallel imaging methods do not produce images with such simple noise characteristics because there are many other complicating factors. Many pMRI methods fully sample the center of *k*-space in order to compute the interpolation weighting factors. Therefore, the sampling density of *k*-space is variable. This further modifies the spatial variability and spatial correlation of image domain noise. In addition, the power of *k*-space pMRI stems from using the relationship of spatial sensitivity between the various coil elements to reduce the amount of data required to complete an image. Therefore, the interpolation spreads the noise from all coil elements into all other coil ele-

ments. Furthermore, the weighting factors used may vary through *k*-space. Finally there is also the influence of the noise correlation matrix Ψ. These and other factors result in a complex and varying spatial noise characteristic that has not, to date, been fully explored and thus far eludes generalizations across receiver coil systems and pMRI processes.

The spatially varying property of noise in pMRI provides an additional motivation to measure image SNR. However, many of the commonly used SNR measurement methods cannot be applied rigorously or appropriately in pMRI. As noted above, any method that computes noise statistics from background regions may produce incorrect results. The only generally viable SNR measurement methods analyze noise in signal regions. In this discussion, it is assumed that the SNR level is sufficiently high so that there is no possibility of signal rectification by the magnitude operation. Small ROI measurements are not advisable either, because short-range spatial correlations may produce anomalous results. Large ROI SNR measurements may be valid, but they do not provide the necessarily spatial detail and, therefore, need to be used judiciously.

For large ROI, general SNR measurements (the "difference of images" method) is the simplest option, but this method is susceptible to system drift issues. The NEMA standard reduces system drift issues by computing the standard deviation of the differences between neighboring points[51]. The difference of neighboring points minimizes the impact of drift by assuming drift causes a spatially slowing varying pattern that can be subtracted out. Other methods that reduce the time difference between the two image acquisitions have also been suggested.

Since small ROIs are not recommended, the only generally viable solution for analyzing small-scale SNR details is by a per-pixel SNR analysis. A basic per-pixel method for computing pMRI SNR is described by Reeder et al.[52]. A large number, *n*, of identical images are collected, and the signal mean and standard deviation at each point are computed. The error in the SD estimate is proportional to $n^{-1/2}$, and thus hundreds of images are required to obtain reasonable estimates. This method is potentially sensitive to system drift. One way to reduce system drift is to apply a high-pass filter to the data in each pixel along the time stack of images to filter out slowly varying system drift components. Another problem with this method is that it is relatively slow, because many acquisitions are required to produce accurate statistics. Furthermore, it is not advisable to reduce the number of acquisitions by pooling the statistics of a few neighboring pixels because of short-range spatial correlation issues in pMRI. Once the mean and standard deviation of each pixel along the time stack of images has been computed, it is a simple procedure to compute image SNR for each pixel using a rudimentary software program. While the high-pass filtering should have eliminated system drift issues on a per-pixel basis, system drift may also cause a slight motion of the apparent phantom position. Therefore, SNR measurements near edges may not be accurate since the signal levels in edge pixels change significantly, causing high standard deviations and low means.

The choice of pulse sequence for measuring SNR is not a trivial concern for pMRI. Traditionally, SNR analysis has often been performed with robust and slow spin echo sequences, impractical for pMRI SNR analyses from the perspective of speed. The sole purpose for a time stack of fast images is to build a per-pixel parametric image of SNR. One can also produce a parametric g-factor map for a given coil-phantom combination from several of these SNR maps obtained using various acceleration factors. Fast gradient echo sequences with lower SNR are required; however, simultaneous measurements of SNR and image resolution may not be possible given the nature of the sequence. Because pMRI SNR testing is not a substitute for the traditional simultaneous SNR and resolution tests, equipment quality control (QC) is not a concern. An alternative approach is to acquire one high-contrast, high-SNR volume of images for visual inspection of subtle artifacts that become more apparent at high SNR, in addition to the multiple series of fast scans. The lower SNR expected from the fast scans

will tend to mask some types of image artifacts. These potential artifacts may also become more obvious in the fast scans if the statistics of mean and standard deviation are presented graphically.

Analyzing a time stack of fast images may be difficult at the MR system console. Some console statistics packages may not have the ability to measure mean and standard deviation on a pixel-by-pixel basis for a large series of images, but other temporal dynamic analysis packages may have the necessary tools and flexibility for such measurements. If no program is available on the console, DICOM transfers and analysis using commercial or freeware PC-based DICOM viewers and image processing environments may be required.

5.2 Measuring Image Intensity Uniformity in pMRI

Uniformity is another important determinant of image quality. Nonuniformities can mask or mimic pathology. These same spatial nonuniformities are also required to provide the spatial discrimination necessary for pMRI methods to work properly. For this reason, the medical device industry has been moving toward developing pMRI-compatible coils with an increasing number of channels or elements. Often, these new coils are comprised of an array of simple surface coils appropriately packaged to cover and encompass the necessary spatial volume. Thus, the need for clinical imaging speed must be balanced against the clinical need for good image uniformity. Some manufacturers provide software functions to help optimize this balance for the end user. Consequently, an image quality metric that can quantify image uniformity is important for MRI systems equipped with pMRI. Since the field of parallel imaging has not yet advanced to the stage where coils are being optimized for specific reconstruction algorithms, this discussion of image uniformity is general to all pMRI methods.

There are several NEMA standards that contain uniformity measurement methods, but MS3-2003 is the only uniformity-specific standard[53]. NEMA MS3-2003 was modified from the previous MS3 standard which was, in turn, adopted from the nuclear medicine gamma camera standard. The NEMA standard seeks the maximum and minimum signal value within the ROI and defines nonuniformity (*NU*) as the difference of the two signal values divided by the sum of the same two values:

$$NU = \frac{|\max - \min|}{|\max + \min|} \tag{15}$$

With the most recent version of the NEMA standard, zero nonuniformity is defined as perfect 100% uniformity (U) where the relationship is:

$$U = 1 - NU \tag{16}$$

The MR literature typically refers to this measure of MR uniformity as the "integral method." Unlike nuclear medicine gamma cameras, there is no integration of signal with time. This name was recently changed in the most recent edition of the standard to "peak difference."

The main disadvantage of the NEMA method is its undue sensitivity to image SNR. As image noise increases, the minimum and maximum signal pixels are driven farther apart, resulting in an apparent lowering of image uniformity. This method is SNR-sensitive because only two pixels from the entire ROI are used. Other uniformity techniques have adapted the NEMA method to derive similar metrics with somewhat less SNR sensitivity (i.e., the ACR technique uses small ROIs to average over outliers that may drive a large difference between min and max pixels). Although nonuniformity of different coil elements is essential for pMRI, in practice, peak-difference NEMA-type methods can only be used with volume coils because the uniformity values from surface coil arrays are so low that the uniformity measure implies the coil is useless. Furthermore, the surface coil array NEMA uniformity results are sensitive to ROI placement because any ROI movement in the region of strong signal

causes dramatic uniformity measurement variations. For these reasons, NEMA has developed other uniformity measurement methods for specific coil situations[54,55]. However, the methods provided in these standards can be cumbersome.

For some of the reasons listed above, the IEC has also adopted a measure of uniformity that is essentially insensitive to SNR[56]. This method has some desirable attributes that are useful for pMRI coils. It uses a measure of image uniformity called the Normalized Absolute Average Deviation (NAAD). The NAAD computes the average of the absolute deviation of each pixel's signal intensity (Y_i) in the ROI from the average signal intensity value of the ROI, $\overline{Y}$. This sum is then normalized by the ROI mean,

$$NU = \frac{1}{N\overline{Y}} \sum_{i=1}^{N} (|Y_i - \overline{Y}|). \tag{17}$$

This measure of uniformity weights the contribution of each pixel in the ROI equally, decreasing the sensitivity to image SNR and ROI position. By considering the contribution of each pixel equally, NAAD can be applied to surface coils and surface coil arrays with reduced ROI position sensitivity of the NEMA method. The NAAD method also produces reasonable uniformity measurements because the equal contribution of each pixel provides a uniformity measure that weighs not only the magnitude of the deviation from a common reference signal level, but the relative distribution of pixel deviations. Surface coils have small regions with intense signal and large regions with lower signal sensitivity. By the NEMA "peak difference" uniformity measurement, uniformity is near zero because the difference between the signals in the two regions is very high. Alternatively, a surface coil could be considered to be relatively uniform because there is a relatively large area of similar signal sensitivity with a small region of intense signal. The NAAD uniformity measure provides a better measure of uniformity in these situations.

The disadvantage of the NAAD method is that it introduces a statistical measure (Absolute Average Deviation) that is not a component of typical medical workstation ROI statistical measurement tools. Thus, the use of this uniformity measure will require off-line processing with special algorithms at this time.

Another potential disadvantage is in the metric itself. Traditionally, uniformity values are bounded in the range [0–1], with "1" representing ideal uniformity (100%). Note that for NAAD, ideal uniformity will have a value of 0 in the ideal, yet hypothetical, case where each pixel value is exactly the same.

Finally, one of the most important qualities of using a particular uniformity measurement during image quality assurance (QA) is its sensitivity to coil performance changes and artifact appearance. NAAD is largely insensitive to inherent surface coil uniformity variations, but the same may also be true with some artifacts, allowing system performance problems to go unnoticed.

5.3 A Practical Protocol for Quality Assurance for pMRI

Given the issues and concerns relating to SNR, uniformity, and artifacts as they pertain to parallel imaging, no standard approach to quality assurance exists that is appropriate for pMRI. For unaccelerated imaging, SNR and uniformity are coupled because of the strong variation in spatial sensitivity for phased-array coils, which is not as important an issue for volume coils. When imaging is accelerated, the relationship between uniformity and SNR becomes more entangled, with spatial correlations or localized variation in noise introduced into an image. Furthermore, unfolding artifacts may be generated that contribute to apparent decreases in SNR and in uniformity, particularly in the case of image-based pMRI methods. Finally, all of these effects will vary in an indeterminate way depending on the pulse sequence that one might wish to use for QA measurements.

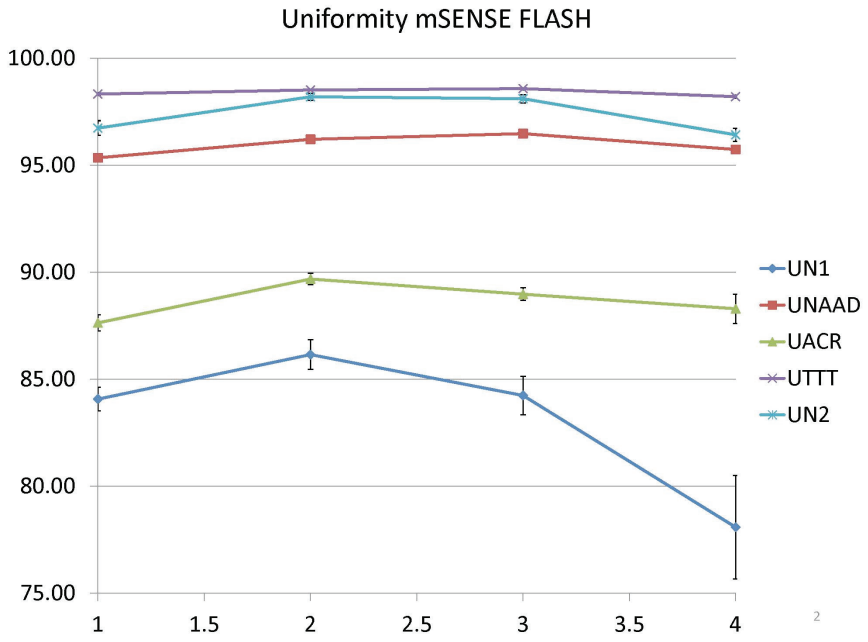

Figure 13. Five different uniformity metrics applied to characterization of images using a FLASH sequence paired with image-based pMRI at different acceleration factors. The different methods are as follows: UN1 = NEMA peak-difference method. UNAAD = NAAD-based uniformity. UACR = ACR uniformity. UTTT and UN2 = uniformity measures proposed by Goerner in reference 57.

Acknowledging the difficulties with measuring SNR and uniformity in pMRI, this Task Group explored the merits of a proposed QA protocol based on a few simple principles. First, because of the inherent problems of uniformity introduced with phased-array coils in general, relative measurements were employed to compare differences between images from non-accelerated and accelerated sequences. Uniformity and SNR were calculated for non-accelerated scans. Then all other uniformity and SNR values were normalized by the non-accelerated scan values. Although this normalization process should de-emphasize some of the dependence of these metrics on phased-array coil signal nonuniformity, some residual dependence may remain. As a result, one should take extra care to ensure reproducible phantom placement in the coil for pMRI.

The possible presence of artifacts and their contribution to uniformity and SNR was ignored in this exercise for simplicity, although artifact detection is clearly an important part of a QA program. Considering the inherent nonuniformity of surface coils, a choice was made between balancing inherent coil nonuniformity and potentially aberrant imaging nonuniformity. Furthermore, simplicity in the uniformity metric was considered. As an example, Figure 13 shows a comparison of five different uniformity measures using a spoiled GRE technique (FLASH), for conventional imaging as well as three different acceleration factors of pMRI. As expected, the NEMA peak-difference method (UN1) displays the largest nonuniformity for all measures, principally from inherent nonuniformity of the coil. Likewise, NAAD-based uniformity (UNAAD) shows better overall uniformity. However, the uniformity variation observed using NAAD as acceleration increases is minimal, even though images anecdotally show increasing nonuniformity from g-factor-related effects. Finally, other metrics (UN2)

show good overall uniformity and sensitivity to acceleration-based increases in nonuniformity. However, UN2 is not quickly calculable, which may render this technique less attractive for QA work.

Considering such issues, uniformity was calculated using the NAAD method as well as the traditional ACR method. Although the inherent nonuniformity of surface coils strictly violates the assumptions of the ACR test (namely, that the coil should perform uniformly), this method is well-known, easily calculable, and sensitive to small differences in nonuniformity.

SNR was measured using a modified version of the NEMA "difference of images" method. Given two images, S_1 and S_2, the sum and difference for each pair of pixels in a location were calculated. Once a measurement ROI was assigned, SNR was determined using the following equation:

$$SNR_{ROI} = \frac{< S_1 + S_2 >_{ROI}}{\sqrt{2}\sigma_{S1-S2}|_{ROI}} \tag{18}$$

Here, σ_{S1-S2} is the standard deviation of pixel differences in the ROI. This method has been demonstrated to correlate well with SNR determined from a series of images collected over time[52], but with less demand for image processing as well as scanner time.

Several duplicate phantoms were constructed and shipped to host institutions of the co-authors. The phantom consisted of a standard #3 soccer ball with a double bladder (Baden Series Z Soccer Ball PN S130Z-018). Each phantom was filled with a solution of 5.45 g NaCl (99.99% pure) and 5.29 ml of Magnevist per 1 L of distilled water. All phantoms were filled from one batch of solution for uniformity. Predicted conductivity and T1 (at 3T) of the solution were 0.023 S/m and 121 msec, respectively. The nominal OD was 18.6–19.4 cm. Filled volumes varied from 2411–2423 ml, with an effective ID of 16.6–16.7 cm.

Scans were acquired on several machines at these institutions. These included Philips, Siemens, and GE MRI systems. Both 1.5T and 3T scanners were used. For brevity, we will present only 3T data. Both fast spin-echo and gradient echo pulse sequences were used.

Automated image analysis proceeded using an in-house MATLAB program written by one of the co-authors (NY). Regions of interest were defined for the analysis in the following manner. Only the center slice for each scan was used during analysis. First, the approximate center of the phantom was found using a coarse segmentation of the phantom by threshold, after which the centroid was determined. Both the uniformity and SNR ROIs were defined as a circular mask 80 pixels in radius (~68.7 mm). This size eliminated a peripheral region of 18 pixels (~15.5 mm) around the phantom edge. In this manner, a large ROI was used to minimize the standard error in the mean measurements, but the boundary was excluded to minimize effects nearest to the phased-array coil.

Figure 14 compares relative SNR values for increasing acceleration between 3T MRI systems of different make and model. Figures 15 and 16 shows a similar comparison for both NAAD and ACR-based uniformity. Qualitatively, the 3T results are similar for 1.5T machines. Absolute SNR values fell in the range of ~120–170 (3T, SE); ~200–280 (3T, GRE); ~30–50 (1.5T, SE); and ~60–100 (1.5T, GRE). Ranges for absolute NAAD values were ~0.8–0.95 (3T, SE); ~0.85–0.95 (3T, GRE); ~0.89–0.9 (1.5T, SE); and ~0.89–0.95 (1.5T, GRE), while ranges for ACR-based uniformity were lower by about ~0.1. As expected, ACR-based uniformity also shows more sensitivity to acceleration, although variation is observed in NAAD as well at higher acceleration values. As acceleration is increased to R=2, variations exist generally across all variables, considering vendor, site, and technique. Assuming the perfect case where g=1 as R increases to 2, the reduction in SNR generally follows Equation 8 (where $SNR_{relative}$ (R=2) should be ~ $1/\sqrt{2}$ $SNR_{relative}$ (R=1), but it also demonstrates that extra gains in SNR arise from the use of shorter echo trains as mentioned previously. For the 32-channel coil, the differences in image-based and k-space-based techniques are clearly demonstrated at higher accelera-

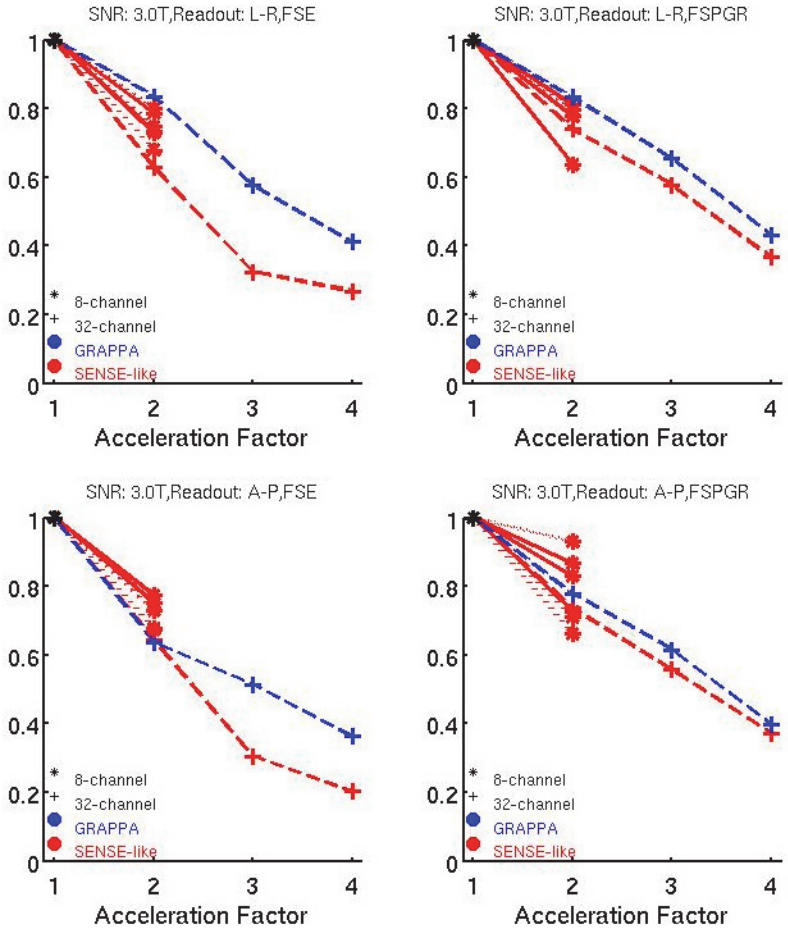

Figure 14. Relative SNR values for FSE and FSPGR sequences, with L-R and A-P readouts. Solid lines represent GE systems, dashed lines represent Siemens systems, and dotted lines represent Philips systems. Red data is from SENSE-based techniques, while blue data is from GRAPPA-based pMRI techniques.

tion factors. Both relative SNR and uniformity values showed a decrease for image-based techniques, most likely due to the more localized nature of SNR decreases and of reconstruction artifacts.

Based on these observations, we make the following suggestions concerning QA procedures specific to pMRI. The choice of SNR and uniformity measurement may affect the sensitivity of QA measurements of pMRI to changes over time. The SNR difference method is currently the best method for measuring SNR, given the nonuniformity of SNR introduced by phased-array coils. Use of this measure will require the medical physicist to invest some time using a basic software tool to subtract images. Tools such as ImageJ[58], a free software that is widely available from the NIH, offer one method for calculation of SNR using the difference method.

Any meaningful uniformity measurement in pMRI should be sensitive to nonuniformities introduced by changes in pMRI performance, while being insensitive to the intrinsic nonuniformity of phased-array coils. The measurement should also be easily performed using commonly available software tools.

The task group did not find a uniformity measure that is appropriate for all pMRI conditions and pulse sequences. It may be that uniformity is not a robust indicator of system performance changes at the present time. *Collecting uniformity measurements for later study and comparison of these with SNR changes is probably the best course of action available currently.*

For institutions that wish to add QA procedures for characterizing pMRI performance, we suggest starting with a parallel-based protocol that is commonly used at that institution, such as a gradient-echo head protocol. Issues of coil performance for other pMRI-enabled coils can be determined with periodic coil SNR testing with ordinary protocols. Using the protocol of interest, two scans should be

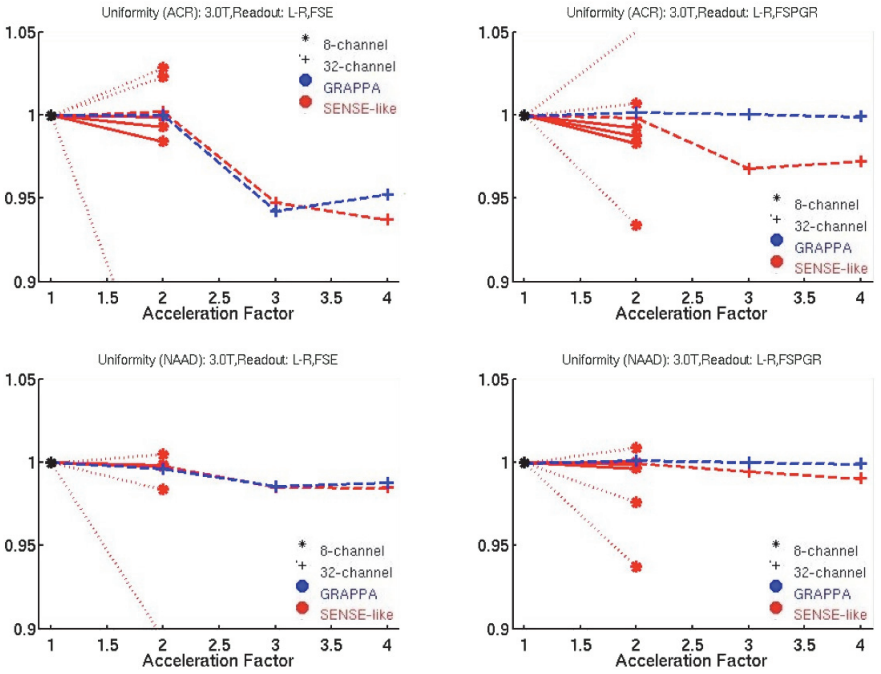

Figure 15. Relative ACR uniformity and NAAD values for FSE and FSPGR sequences, with an L-R readout. Solid lines represent GE systems, dashed lines represent Siemens systems, and dotted lines represent Philips systems. Red data is from SENSE-based techniques, while blue data is from GRAPPA-based pMRI techniques.

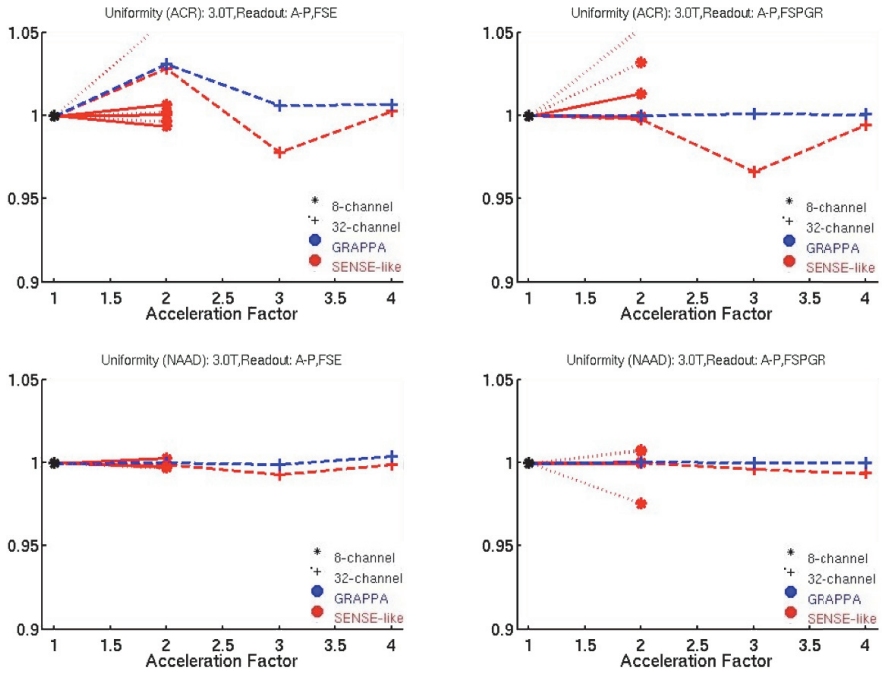

Figure 16. Relative ACR uniformity and NAAD values for FSE and FSPGR sequences, with an A-P readout. Solid lines represent GE systems, dashed lines represent Siemens systems, and dotted lines represent Philips systems. Red data is from SENSE-based techniques, while blue data is from GRAPPA-based pMRI techniques.

acquired with pMRI turned off and two more should be acquired with pMRI turned on to an acceleration factor characteristic of the usage by the institution. For example, if an acceleration factor of R=1.75 is used by that institution, this is the acceleration factor that should be chosen. Note that the protocol should be one that ordinarily produces images of reasonable quality, so it is important to check with the vendor to ensure that the protocol is optimized and not being used in a manner inconsistent with pMRI (e.g., an eight-channel system with acceleration factor, R>2, may produce low-quality images).

Finally, we suggest that the medical physicist should monitor changes in SNR for the pMRI scan relative to the unaccelerated scan. This is most easily accomplished by dividing the SNR of the pMRI scan by the unaccelerated scan. In this manner, absolute changes in SNR that may not affect pMRI directly are not the focus of this particular testing. If values of SNR dramatically change on one given day, one should default to inspecting the individual images for noticeable artifact or spatial increases in noise that appear more marked, to decide whether a problem has developed and how to proceed.

6. Advanced Developments in pMRI

Although parallel imaging was first implemented about 10 years ago, the technique has undergone rapid improvements during this short period of time. The first 10 years has ushered in the use of acceleration factors greater than two, improved methods for calibrating the coil sensitivity[16], and the development of many robust reconstruction methods[59]. Future refinements will allow for a more widespread use of parallel imaging in the clinic. Current areas of research interest include increased numbers of receiver channels, acceleration of three-dimensional (3D) image acquisition, and acceleration of image acquisition in a dynamic time series.

6.1 Three-dimensional pMRI

Cartesian undersampling in 2D imaging can be generalized to 3D imaging, where data within *k*-space can be undersampled along both phase-encode directions in *k*-space. The corresponding acceleration rate, R_{2D}, for acquiring an image volume is the product of rates along each phase-encode direction, $R_x \times R_y$, leading to a substantial time-savings, even for low acceleration factors along each direction. This technique is especially attractive because the g-factor (and, consequently, SNR) does not drop off as rapidly with increased R values in 3D imaging using 2D-pMRI (Figure 17). Parallel imaging in 3D has been implemented using image-based techniques[60] and hybrid techniques that employ both image-based and *k*-space-based reconstruction to alleviate the computational load of *k*-space techniques but benefit from their noise properties. Although the problem of regional noise enhancement

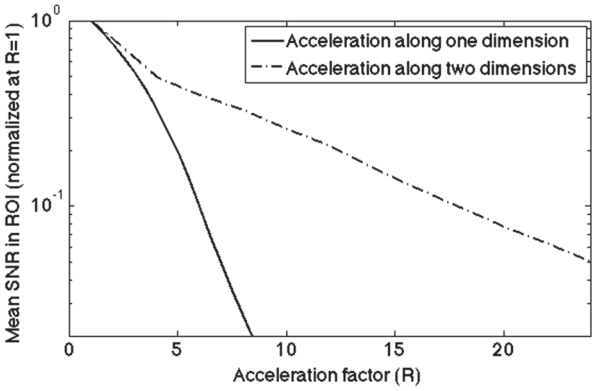

Figure 17. Maximum achievable SNR at center of elliptical volume of tissue as a function of acceleration factor (R) with 32-element coil, comparing acceleration along one and two phase-encoding directions. Adapted from reference 34.

using image-based techniques is generally improved in 3D, the aliasing becomes rather difficult to understand[61]. Therefore, simulation is rather important for design optimization of 3D parallel imaging coils. Furthermore, this optimization will not necessarily be applicable for all anatomical procedures. The 2D-pMRI packages are available on all high-end MRI systems.

In addition to improved 3D imaging, one important potential application of 3D parallel imaging techniques is the rapid acquisition of 2D spectra[62]. Because 2D spectroscopy is analogous to 3D imaging—with both using two spatial phase encodings and a temporal readout dimension—data along both axes in *k*-space can be undersampled for a dramatic reduction in spectral acquisition time. Spectroscopy is a good candidate for accelerated acquisition times, considering that many 2D spectroscopic sequences have a high SNR without pMRI.

6.2 Parallel MRI at High Magnetic Field Strengths

When pMRI is used to reduce the total number of RF pulses used for a particular acquisition, it automatically reduces the scanning limitations imposed by specific absorption rate (SAR) of RF energy. Fewer RF pulses per acquisition leads to a lower amount of RF-based heating over the duration of a given scan. This feature of pMRI is particularly useful when imaging at magnetic fields of 3T or higher, because SAR increases as the square of the resonant frequency and can become prohibitive when using sequences that employ a large number of high flip-angle pulses, such as fast spin echo. Recent studies[59] also suggest that SNR losses at high acceleration factors will be much less using pMRI at high resonant frequencies (high B_o) (Figure 18).

6.3 Non-Cartesian Methods for MR Image Acceleration

Our general discussion of parallel imaging has focused on the reconstruction of 2D images after acquiring some fraction of phase-encoding lines in *k*-space, using a Cartesian sampling scheme. In general, undersampling need not occur exclusively along the phase-encode encoding direction and can take place in any configuration across *k*-space. For example, a non-Cartesian method like spiral scanning undersamples data along its spiral trajectory, leading to a dataset in *k*-space that is sparse along both the x- and y-axis of a Cartesian grid[63]. Considering only Cartesian sampling in this discussion, undersampling along the frequency-encoding direction does not lead to a reduction in image acquisition time and is, therefore, not used. With an image-based parallel technique, it should be noted that the use of large acceleration factors with undersampling along one direction can quickly lead to regionally concentrated noise enhancement[64]. Work to alleviate this problem is ongoing, including

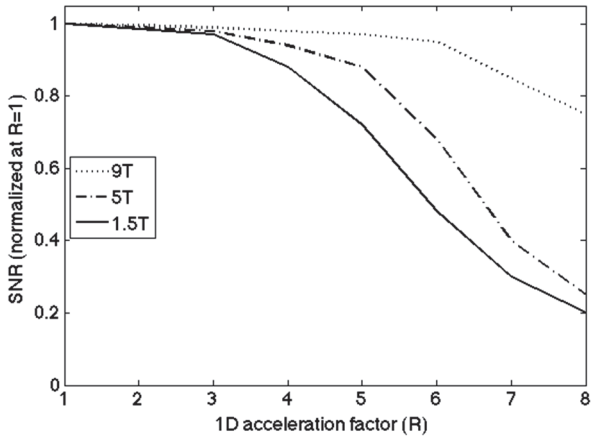

Figure 18. SNR values for a theoretical right elliptical cylinder with the electrical properties of liver imaged using parallel technique. The graph shows the dependence of SNR on acceleration factor for Bo-fields ranging from 1.5T to 9T at point at the center of sample, normalized so that SNR=1 when R=1. Adapted from reference 63.

advanced reconstruction techniques[65] and multi-slice parallel imaging with phase-shifting of the RF excitation pulse from slice to slice[60,66] to produce more uniformity in aliasing artifacts[67]. In the use of 2D images in constructing a three-dimensional image volume, parallel imaging accelerates the image volume acquisition by the 2D acceleration factor, R_{2D}, regardless of the number of slices. As noted in a previous section, 2D acceleration "spreads out" the noise more evenly for image-based pMRI techniques.

Thus there is currently great interest in what have generally been classified as "non-Cartesian" methods for parallel imaging[68–71]. These methods employ complex k-space trajectories which, depending on the specific applications, may sample certain regions of *k*-space with lesser or greater density. However, these approaches require complex image reconstruction algorithms and very powerful image processing hardware.

6.4 Parallel Imaging Framework for RF Excitation: Transmit SENSE

The basis of parallel imaging is that data collected using an array of coil elements with overlapping spatial sensitivity contain redundant spatial information, and that judicious undersampling of this information allows for a reduction in scan time without a loss of spatial information. This concept can be extended from signal reception to RF excitation, in which each coil element in an array contributes, in part, to excitation of the tissue of interest. This novel technique[72,73] has been named "Transmit SENSE."

To understand Transmit SENSE, one must remember how RF excitation proceeds and how to specify a spatially selective excitation. For a typical 2D imaging sequence, the application of a linear "slice-select" gradient and an oscillating RF field, $B_1(t)$, causes excitation of a slice of tissue. The shape of the waveform, or "envelope," of $B_1(t)$ results in a spectrum of excitation frequencies, which can be determined using a Fourier transform. By using the gradient to specify that the excitation frequency depends on position along the slice-select direction, one can create transverse magnetization along that direction in proportion to the frequency spectrum of $B_1(t)$. Typically, a sinc-like envelope is used, which results in a fairly uniform spectrum of frequencies within a limited bandwidth, and few frequencies excited outside the band. This uniform spectrum within a limited band yields a rectangular spatial profile of excited nuclei. Expanding on this idea, one can create a very complicated spatial excitation pattern by using a time-varying gradient, G(t), and a suitable waveform, $B_1(t)$. Navigator pulses for motion detection are one common example of spatially selective pulses. To determine the appropriate waveform for $B_1(t)$, one must first Fourier transform the desired spatial excitation pattern $F(\mathbf{r})$ into the frequency domain $f(\mathbf{k})$. By adjusting the gradients $G_{x,y,z}(t)$, one can formulate the excitation process within a FOV as traveling along a *k*-space trajectory, $\mathbf{k}(t)$, analogous to MR reception (as per Equation 8). In principle, a great deal of flexibility in tailoring an RF excitation pulse exists. However as the desired excitation patterns become more complex, the duration of the RF excitation pulse also becomes unmanageably long.

We can extend this analogy to parallel imaging, which is based on MR reception. If excitation can be thought of as a traversal of *k*-space, then multiple coils could, in theory, traverse different sub-samples of this *k*-space, additively sampling the same total region in *k*-space. Since each sub-sampled traversal is smaller in area, the duration of each excitation can be correspondingly smaller as well. One can reduce the transmit duration by an acceleration factor analogous to parallel imaging. To use multiple coils, one must decompose the excitation pattern into a sum of individual patterns desired from each coil, weighted by the corresponding sensitivity profiles of the individual coil elements.

Transmit-SENSE is now used routinely in the clinic, but it requires hardware that allows for multiple, decoupled transmission via excitation coil elements. Coil design is not only critical in decoupling but also in SAR remediation[74,75]. Due to its novelty, areas of clinical applicability for Transmit

SENSE have not been fully explored at this time. An important area of application of Transmit SENSE is to compensate for dielectric effects, which can cause anomalous regions of low signal in high-field MRI systems[76–78]. Other possible benefits of this technology include faster 3D RF pulses, the suppression of susceptibility artifacts in T2* imaging[79], more efficient spectral-spatial RF pulses[80], and the compensation of blood in-flow effects in MRA[81].

7. Summary

This report has reviewed many of the technical details associated with pMRI, keeping the goal in mind of educating the medical physicist about challenges and limitations of using this technique. Although the basis of pMRI involves the reduction of the number of phase encodings, multiple implementations exist, including the extension of undersampling into the temporal dimension for a dynamic image series. Although the choice of whether to use an image-based or *k*-spaced-based approach (or some hybrid of the two) may appear arbitrary, knowledge of the inherent performance characteristics for each technique is required for optimal solution of an imaging task. Important questions in this area include "Is the FOV small or within the torso?" and "Is hardware-based reconstruction speed a limitation?"

When confronting a non-diagnostic pMRI image from a poorly optimized protocol, the medical physicist should be able to provide some degree of insight on how to improve the protocol. For instance, the medical physicist should be able to determine how fast of an acceleration factor can be chosen reliably for a given coil, knowing the number of coil elements and configuration. When involved in purchasing decisions, the medical physicist should be able to reasonably compare two different coils that could serve similar clinical functions. The medical physicist should understand the interplay between SNR, acceleration factor, geometric distortion, blurring, resolution, and scan time in a pMRI sequence. The medical physicist should be able to describe the clinical circumstances under which one of these parameters should be increased at the expense of others, with minimal impact to the image quality. The medical physicist should know when it is appropriate to turn off pMRI given the technical limitations. The physicist should be prepared to communicate why some of these basic choices are appropriate to radiology residents and to radiologists.

Critically, pMRI expands the complexity of characterizing system performance and image quality. The medical physicist should be able to provide an explanation of why certain pMRI-based artifacts occur and how to correct for them. As system performance changes over time, a particular QA procedure should be identified as sensitive enough to detect that change. If a test is too sensitive, the detection of small changes in scanner performance may occur with no apparent degradation of diagnostic image quality. Sensitivity may be affected by using phased-array coils with different numbers of elements. Marginally poor coil elements may degrade pMRI images, which may not cause a problem with conventional imaging.

As pMRI continues to evolve, the theoretical complexity of each protocol will also increase. This evolution will likely result in increasing diversity of artifacts. For this reason, continuing education of the medical physicist will be an important component of ensuring good pMRI performance at an institution.

8. References

1. A. Kumar, D. Welti, R.R. Ernst. "NMR Fourier Zeugmatography." *J. Magn. Reson.* **18**:69–83 (1975).
2. P. Mansfield, A.A. Maudsley. "Planar Spin Imaging by NMR." J. Magn. Reson. **27**:101–119 (1977).

3. W.A. Edelstein, J.M.S. Hutchison, G. Johnson, T. Redpath. "Spin Warp Imaging and Applications to Human Whole Body Imaging." *Phys. Med. Biol.* **25**:751–756 (1980).
4. D.B. Twieg. "The k-Trajectory Formulation of the NMR Imaging Process with Applications in Analysis and Synthesis of Imaging Methods." *Med. Phys.* **10**:610–621 (1983).
5. S. Ljuggren. "A Simple Graphical Representation of Fourier-Based Imaging Methods." *J. Magn. Reson.* **54**:338–343 (1983).
6. J.M. Pauly, D.G. Nishimura, A.A. Macovski. "A k-Space Analysis of Small Tip-Angle Excitation," *J. Magn. Reson.* **81**:43–56 (1989).
7. M. Hutchinson, U. Raff. "Fast MRI Data Acquisition Using Multiple Detectors." *Magn. Reson. Med.* **6**:87–91 (1988).
8. D. Kwiat, S. Einav, G. Navon. "A Decoupled Coil Detector Array for Fast Image Acquisition in Magnetic Resonance Imaging." *Med. Phys.* **18**:251–265 (1991).
9. J.B. Ra, C.Y. Rim. "Fast Imaging Using Sub-encoding Data Sets from Multiple Detectors." *Magn. Reson. Med.* **30**:142–145 (1993).
10. J.W. Carlson, T. Minemura. "Imaging Time Reduction through Multiple Receiver Coil Data Acquisition and Image Reconstruction." *Magn. Reson. Med.* **29**:681–688 (1993).
11. K.P. Pruessmann, M. Weiger, M.B. Scheidegger, P. Boesiger. "SENSE: Sensitivity Encoding for Fast MRI." *Magn. Reson. Med.* **42**:952–962 (1999).
12. K.P. Pruessmann. *Sensitivity Encoded Magnetic Resonance Imaging* (Ph.D. thesis). Swiss Federal Institute of Technology, Zurich (2000).
13. D.K. Sodickson, W.J. Manning. "Simultaneous Acquisition of Spatial Harmonics (SMASH): Fast Imaging with Radiofrequency Coil Arrays." *Magn. Reson. Med.* **38**:591–603 (1997).
14. D.K. Sodickson, M.A. Griswold, P.M. Jakob. "SMASH Imaging." *Magn. Reson. Imag. Clin. North Amer.* **7**:1–18 (1999).
15. M.A. Griswold, et al. "Generalized auto calibrating partially parallel imaging (GRAPPA)." *Magn. Reson. Med.* **47**:1202–1210 (2002).
16. W.E. Kyriakos, et al. "Sensitivity Profiles from an Array of Coils for Encoding and Reconstruction in Parallel (SPACE RIP)." *Magn. Reson. Med.* **44**:301–308 (2000).
17. D.K. Sodickson, C.A. McKenzie. "A Generalized Approach to Parallel Magnetic Resonance Imaging." *Med. Phys.* **28**:1629–1643 (2001).
18. M. Bydder, D.J. Larkman, J.V. Hajnal. "Generalized SMASH Imaging." *Magn. Reson. Med.* **47**:160–170 (2002).
19. Y. Machida, S. Uchizono, N. Ichinose. "Fold-Over Aliasing Artifact Suppression Technique in MRI Parallel Imaging: Considerations of Role of FOV in Image Formation Procedure." *Proc. Intl. Soc. Mag. Reson. Med.* 506 (2005).
20. M. Weiger, et al. "Sensitivity Encoding as a Means of Enhancing the SNR Efficiency in Steady-state MRI." *Magn. Reson. Med.* **53**:177–185 (2005).
21. M. deVries, et al. "Contrast-enhanced Peripheral MR Angiography Using SENSE in Multiple Stations: Feasibility Study." *J. Magn. Reson. Imag.* **21**:37–45 (2005).
22. J.F. Glockner, et al. "Parallel MR Imaging: a User's Guide." *Radiographics* **25**:1279–1297 (2005).
23. C.J. Zech, et al. "High Resolution Imaging of the Liver with T2-weighted Sequences Using Integrated Parallel Imaging: A Comparison of Prospective Motion Correction and Respiratory Triggering." *J. Magn. Reson. Imag.* **20**:443–450 (2004).
24. M. Augustin, F. Fazekas, R. Bammer. "Fast Patient Workup in Acute Stroke Using Parallel Imaging." *Top. Magn. Reson. Imag.* **15**:207–219 (2004).

25. B. Madore, G.H. Glover, N.J. Pelc. "Unaliasing by Fourier-Encoding the Overlaps Using the Temporal Dimension (UNFOLD), Applied to Cardiac Imaging and fMRI." *Magn. Reson. Med.* **42**:813–828 (1999).
26. M.A. Guttman, et al. "Real-time Accelerated Interactive MRI with Adaptive TSENSE and UNFOLD." *Magn. Reson. Med.* **50**:315–321 (2003).
27. J. Tsao, P. Boesiger, K.P. Pruessmann, "k-t- BLAST and k-t SENSE: Dynamic MRI with High Frame Rate Exploiting Spatiotemporal Correlations." *Magn. Reson. Med.* **50**:1031–1042 (2003).
28. F. Huang, et al. "*k-t* GRAPPA: a k-space Implementation for Dynamic MRI with High Reduction Factor." *Magn. Reson. Med.* **54**:1172–1184 (2005).
29. C. Baltes, et al. "Accelerating Cine Phase-contrast Flow Measurements Using *k-t* BLAST and *k-t* SENSE." *Magn. Reson. Med.* **54**:1430–1438 (2005).
30 T. Chung, R. Muthupillai. "Application of SENSE to Clinical Pediatric Body Imaging." *Top. Magn. Reson. Imag.* **15**:187–196 (2004).
31. C.E. Hayes, L. Axel. "Noise Performance of Surface Coils for Magnetic Resonance Imaging at 1.5 T." *Med. Phys.* **12**:605–607 (1985).
32. J.W. Murakami, C.E. Hayes, E. Weinberger. "Intensity Correction of Phased-array Surface Coils." *Magn. Reson. Med.* **35**:585–590 (1996).
33. J.S. Hyde, et al. "Parallel Image Acquisition from Non-interacting Local Coils." *J. Magn. Reson.* **70**:512–517 (1986).
34. PIN Diode Circuit Designers Handbook. Microsemi-Watertown, 1992. Downloadable from: http://www.microsemi.com/literature/pinhandbook.pdf.
35. B. Doherty. Micronote 711, Analysis of NMR/MRI Coils Using PIN Diode Switches. Downloadable from: http://www.microsemi.com/micnotes/711.pdf.
36. Y. Zhu, et al. "Highly Parallel Volumetric Imaging With a 32-Element RF Coil Array." *Magn. Reson. Med.* **52**:869–877 (2004).
37. M.A. Ohliger, P. Ledden, C.A. McKenzie, D.K. Sodickson. "Effects of Inductive Coupling on Parallel MR Image Reconstructions." *Magn. Reson. Med.* **52**:628–639 (2004).
38. D.K. Sodickson, et al. "Rapid Volumetric MRI Using Parallel Imaging with Order-of-magnitude Accelerations and a 32-element RF Coil Array: Feasibility and Implications." *Acad. Radiol.* **12**:626–635 (2005).
39. M. Weiger, K.P. Pruessmann, P. Boesiger. "2D SENSE for Faster 3D MRI." *MAGMA* **14**:10–19 (2002).
40. G.C. Wiggins, et al. "A 96-channel MRI System with 23- and 90-channel Phased Array Head Coils at 1.5 Tesla." *Proc. Intl. Soc. Mag. Reson. Med.*:671 (2005).
41. M.P. McDougall, S.M. Wright. "64-channel Array Coil for Single Echo Acquisition Magnetic Resonance Imaging." *Magn. Reson. Med.* **54**:386–392 (2005).
42. J.W. Goldfarb. "The SENSE Ghost: Field-of-view Restrictions for SENSE Imaging." *J. Magn. Reson. Imag.* **20**:1046–1051 (2004).
43. M.A. Griswold, et al. "Field-of-view Limitations in Parallel Imaging." *Magn. Reson. Med.* **52**:1118–1126 (2004).
44. C. Preibisch, et al. "Comparison of Parallel Acquisition Techniques Generalized Autocalibrating Partially Parallel Acquisitions (GRAPPA) and Modified Sensitivity Encoding (mSENSE) in Functional MRI (fMRI) at 3T." *J. Magn. Reson. Imag.* **27**:590–598 (2008).
45. S. Skare, et al. "Clinical Multishot DW-EPI through Parallel Imaging with Considerations of Susceptibility, Motion, and Noise." *Magn. Reson. Med.* **57**:881–890 (2007).
46. Y.A. Bhagat, et al. "Comparison of Generalized Autocalibrating Partially Parallel Acquisitions and Modified Sensitivity Encoding for Diffusion Tensor Imaging." *Am. J. Neuroradiol.* **28**:293–298 (2007).

47. S.O. Rice. “Mathematical Analysis of Random Noise.” *Bell Sys. Tech. J.* **23**:282–332 (1945).
48. H. Gudbjartsson, S. Patz. “The Rician Distribution of Noisy MRI Data.” *Magn. Reson. Med.* **34**:910–924 (1995).
49. F. Wiesinger, P. Boesinger, K.P. Pruessmann. “Electrodynamics and Ultimate SNR in Parallel MR Imaging.” *Magn. Reson. Med.* **52**:376–390 (2004).
50. D.J. Larkman, et al. “Beyond the G-factor Limit in Sensitivity Encoding Using Joint Histogram Entropy.” *Magn. Reson. Med.* **55**:153–160 (2006).
51. NEMA MS1-2008. “Determination of Signal-to-Noise Ratio (SNR) in Diagnostic Magnetic Resonance Images.” Roslyn VA: National Electrical Manufacturers Association, 2000.
52. S.B. Reeder, et al. “Practical Approaches to the Evaluation of Signal-to-noise Ratio Performance with Parallel Imaging: Application with Cardiac Imaging and a 32-channel Cardiac Coil.” *Magn. Reson. Med.* **54**:748–754 (2005).
53. NEMA MS3-2003. “Determination of Image Uniformity in Diagnostic Magnetic Resonance Images.” Roslyn VA: National Electrical Manufacturers Association, 2003.
54. NEMA MS6-1991 (R2000). “Characterization of Special Purpose Coils for Diagnostic Magnetic Resonance Images.” Roslyn VA: National Electrical Manufacturers Association, 2000.
55. NEMA MS9-2001. “Characterization of Phased Array Coils for Diagnostic Magnetic Resonance Images.” Roslyn VA: National Electrical Manufacturers Association, 2001.
56. IEC 62464-1. “Magnetic Resonance Equipment for Medical Imaging-Part 1: Determination of Essential Image Quality Parameters.” Geneva, Switzerland: International Electrotechnical Commission, 2007.
57. F. Goerner, “Evaluation of Image Quality in Magnetic Resonance Imaging with Partially Parallel Imaging Methods,” Ph.D. thesis (2011).
58. C.A. Schneider, W.S. Rasband, K.W. Eliceiri/ “NIH Image to ImageJ: 25 Years of Image Analysis.” *Nat. Methods* **9**:671–675 (2012).
59. K.P Pruessmann, M. Weiger, P. Borner, P. Boesiger. “Advances in Sensitivity Encoding with Arbitrary k-space Trajectories.” *Magn. Reson. Med.* **46**:638–651 (2001).
60. F.A. Breuer, et al “Controlled Aliasing in Parallel Imaging Results in Higher Acceleration (CAIPIRINHA) for Multi-Slice Imaging.” *Magn. Reson. Med.* **53**:684–691 (2005).
61. U. Dydak, et al. “Sensitivity-Encoded Spectroscopic Imaging.” Magn. Reson. Med. **46**:713–722 (2001).
62. M.A. Ohliger, A.K. Grant, D.K. Sodickson. “Ultimate Signal-to-noise Ratio for Parallel MRI: Electromagnetic Field Considerations.” *Magn. Reson. Med.* **50**:1018–1030 (2003).
63. D.C. Peters, et al. “Undersampled Projection Reconstruction Applied to MR Angiography.” *Magn. Reson. Med.* **43**:91–101 (2000).
64. K.K. Vigen, et al. “Undersampled Projection-reconstruction Imaging for Time-resolved Contrast-enhanced Imaging.” *Magn. Reson. Med.* **43**:170–176 (2000).
65. M. Blaimer, et al. “Virtual Coil Concept for Improved Parallel MRI Employing Conjugate Symmetric Signals.” *Magn. Reson. Med.* **61**:93–102 (2009).
66. K. Setsompop, et al. “Blipped-Controlled Aliasing in Parallel Imaging for Simultaneous Multislice Echo Planar Imaging with Reduced G-factor Penalty.” *Magn. Reson. Med.* **67**:1210–1224 (2012).
67. K.L. Wright et al. “Clinical Evaluation of CAIPIRINHA: Comparison Against a GRAPPA Standard.” *J. Magn. Reson. Imag.* **39**:189–194 (2014).
68. D.B. Tweig. “Parsing Local Signal Evolution Directly from a Single-shot MRI Signal: A New Approach for fMRI.” *Magn. Reson. Med.* **50**:1043–1052 (2003).
69. E.N. Yeh, et al. “Inherently Self-calibrating Non-Cartesian Parallel Imaging.” *Magn. Reson. Med.* **54,** 1–8 (2005).

70. M.S. Hansen, et al. "*k-t* BLAST Reconstruction from Non-Cartesian *k-t* Space Sampling." *Magn. Reson. Med.* **55**:85–91 (2006).
71. C.A. Mistretta, et al. "Highly Constrained Backprojection for Time-Resolved MRI." *Magn. Reson. Med.* **55**:30–40 (2006).
72. D.I. Hoult, G. Kolansky, D. Kripiakevich, S.B. King. "The NMR Multi-transmit Phased Array: A Cartesian Feedback Approach." *J. Magn. Reson.* **171**:64–70 (2004).
73. U. Katscher, P. Börnert, J.S. van den Brink. "Theoretical and Numerical Aspects of Transmit SENSE." *IEEE Trans. Med. Imag.* **23**:520–525 (2004).
74. G. Adriany, et al. "Transmit and Receive Transmission Line Arrays for 7 Tesla Parallel Imaging." *Magn. Reson. Med.* **53**:434–445 (2005).
75. U. Katscher, J. Röhrs, P. Börnert. "Basic Considerations on the Impact of the Coil Array on the Performance of Transmit SENSE." *MAGMA* **18**:81–88 (2005).
76. Z. Zhang, et al. "Reduction of Transmitter B1 Inhomogeneity with Transmit SENSE Slice-Select Pulses." *Magn. Reson. Med.* **57**:842–847 (2007).
77. C.G. Filippi, et al. "Improvements in Lumbar Spine MRI at 3T Using Parallel Transmission." *Am. J. Radiol.* **199**:861–867 (2012).
78. W.A. Willinek, et al. "Dual-Source Parallel Radiofrequency Excitation Body MR Imaging Compared with Standard MR Imaging at 3.0T: Initial Clinical Experience." *Radiology* **256**:966–975 (2010).
79. W. Deng, et al. "Simultaneous z-Shim Method for Reducing Susceptibility Artifacts with Multiple Transmitters." *Magn. Reson. Med.* **61**:255–259 (2009).
80. C. Yang, et al. "Four-Dimensional Spectral-Spatial RF Pulses for Simultaneous Correction of B1+ Inhomogeneity and Susceptibility Artifacts in T2*-Weighted MRI." *Magn. Reson. Med.* **64**:1–8 (2010).
81. C. Roberts, et al. "The Effect of Blood Inflow and B(1)-field Inhomogeneity on Measurement of the Arterial Input Function in Axial 3D Spoiled Gradient Echo Dynamic Contrast-Enhanced MRI." *Magn. Reson. Med.* **65**:108–119 (2011).